https://ntrs.nasa.gov/search.jsp?R=20110016345 2019-08-30T17:36:31+00:00Z

Experimental Validation of $\mathcal{L}_1$ Adaptive Control: Rohrs' Counterexample in Flight

Enric Xargay*
University of Illinois at Urbana-Champaign, Urbana, IL 61801

Vladimir Dobrokhodov†
Naval Postgraduate School, Monterey, CA 93943

Naira Hovakimyan‡
University of Illinois at Urbana-Champaign, Urbana, IL 61801

Isaac Kaminer§, Ioannis Kitsios¶
Naval Postgraduate School, Monterey, CA 93943

Chengyu Cao ‖
University of Connecticut, Storrs, CT 06269

Irene M. Gregory **
NASA Langley Research Center, Hampton, VA 23681

Lena Valavani ††
Hellenic Space Systems S.A., Athens, Greece

The paper presents new results on the verification and in–flight validation of an $\mathcal{L}_1$ adaptive flight control system, and proposes a general methodology for verification and validation of adaptive flight control algorithms. The proposed framework is based on Rohrs' counterexample, a benchmark problem presented in the early 80s to show the limitations of adaptive controllers developed at that time. In this paper, the framework is used to evaluate the performance and robustness characteristics of an $\mathcal{L}_1$ adaptive control augmentation loop implemented onboard a small unmanned aerial vehicle. Hardware–in–the–loop simulations and flight test results confirm the ability of the $\mathcal{L}_1$ adaptive controller to maintain stability and predictable performance of the closed loop adaptive system in the presence of general (artificially injected) unmodeled dynamics. The results demonstrate the advantages of $\mathcal{L}_1$ adaptive control as a *verifiable* robust adaptive control architecture with the potential of reducing flight control design costs and facilitating the transition of adaptive control into advanced flight control systems.

Nomenclature

$r(t)$	turn rate seen by the adaptive augmentation loop (affected by unmodeled dynamics)
$r_{\text{cmd}}(t)$	turn rate reference signal
$r_{\text{m}}(t)$	turn rate output response of the reference model to $r_{\text{cmd}}(t)$
r_{ad}	turn rate adaptive control signal sent to the onboard autopilot

*Doctoral Student, Department of Aerospace Engineering, Student Member AIAA; xargay@illinois.edu.
†Research Assistant Professor, Department of Mechanical & Aerospace Engineering, Senior Member AIAA; vldobr@nps.edu.
‡Professor, Department of Mechanical Science and Engineering, Associate Fellow AIAA; nhovakim@illinois.edu.
§Professor, Department of Mechanical & Aerospace Engineering, Senior Member AIAA; kaminer@nps.edu.
¶Postdoctoral Research Fellow, Department of Mechanical & Aerospace Engineering, Cpt (HAF); ikitsios@nps.edu.
‖Assistant Professor, Department of Mechanical Engineering, Member AIAA; ccao@engr.uconn.edu.
**Senior Research Engineer, Dynamic Systems and Controls Branch, Associate Fellow AIAA; irene.m.gregory@nasa.gov.
††President, Hellenic Space Systems S.A., Associate Fellow AIAA; valavani@mit.edu.

I. Introduction

Inner loop adaptive flight control systems (FCSs) may provide the opportunity to improve aircraft performance and reduce pilot's workload at challenging flight envelope conditions or in the event of severe control surface failures and vehicle damage. However, implementation of adaptive control technologies can increase the complexity of FCSs beyond the capability of current Verification and Validation (V&V) processes. This fact, combined with the criticality of inner loop flight control systems, appears as a major impediment for the transition of these technologies to military and commercial applications. Programs like NASA's "Integrated Resilient Aircraft Control" (IRAC) and Wright–Patterson AFRL's "Certification Techniques for Advanced Flight Critical Systems" (CerTA FCS) represent an effort to advance the state–of–the–art in the adaptive control technology, to analyze the deficiencies of current V&V practices, and to advance airworthiness certification of adaptive flight control systems.

A good overview on verification, validation, and certification challenges for the transition of adaptive control to safety–critical aerospace applications can be found in [1,2]. In particular, the key hurdles for certification of adaptive flight control systems are (*i*) the lack of *predictability* in the closed loop response; (*ii*) the limited analysis framework for *robustness and performance guarantees* for closed loop adaptive systems; and (*iii*) the lack of *systematic design guidelines* to solve the trade off between adaptation, performance, and robustness. These limitations seem to be directly related to the *asymptotic* nature of the results obtained in the development of the theory of adaptive control over the years. In this sense, it is important to emphasize that, when dealing with practical applications, features such as boundedness, ultimate boundedness, or even asymptotic convergence, are *weak* properties for nonlinear adaptive feedback systems. Much stronger guarantees are needed. On the one hand, performance requirements demand predictable and consistent response of the closed loop system, dependent upon changes in system dynamics and reference signals. On the other hand, unmodeled dynamics, latencies, disturbances, and noise require precise quantification of the robustness and the stability margins of the feedback loop. Moreover, the lack of analytical quantification of the relationship between the adaptation process, the transient response, and robustness margins makes the design of adaptive controllers an overly challenging problem, which is being commonly resolved by either computationally expensive Monte–Carlo simulations or trial and error methods following some empirical guidelines or engineering intuition.

In fact, several examples have been presented over the years to illustrate these limitations. The lack of robustness exhibited by conventional model reference adaptive controllers was first pointed out in 1978 by Egardt[3] and later analyzed in detail by Rohrs et al.[4,5] In particular, Rohrs and coauthors constructed a counterexample where a first order stable plant with two (apparently "harmless") highly damped unmodeled poles was going unstable when driven by a reference sinusoid at the phase crossover frequency or affected by unmeasurable output disturbances at any frequency. The lack of robustness of adaptive controllers has also been analyzed in robust control literature. In [6], Georgiou et al. proved that a conventional parameter adaptive controller has zero robustness margin in the gap metric and can be destabilized by arbitrarily small perturbations in the gap. On the other hand, the lack of transient characterization of (globally) asymptotically stable adaptive controllers was demonstrated by several counterexamples that appeared in the literature.[7–12] These examples showed that the system output can have very poor transient tracking behavior before ideal asymptotic convergence takes place. In this sense, Zang et al.[13] suggested the need to quantify transient response and derive performance bounds for closed loop adaptive systems.

Especially, the results and conclusions of Rohrs' counterexample presented in [4] (and in its journal version [5]) led to an ideological controversy and, as a consequence, robustness and convergence of adaptive controllers started to be investigated by other authors. A thorough explanation for the phenomena observed in Rohrs' simulations was provided in papers by Åström[14,15] and Anderson.[16] Other authors attempted to provide a solution to the problem of parameter drift with limited success, as the modifications they proposed were essentially compromising the adaptation process in varying degrees, and, ultimately, could not always predictably prevent the parameter drift.[17–22] The basic idea of all the modifications was to limit the gain of the adaptation loop and to eliminate its integral action. Examples of these modifications are the σ–modification[21] and the e–modification.[22] A good survey on the topic can be found in [23]. While all these modifications offered some improvement vis a vis the robustness, none of them provided the capabilities to (*i*) quantify the transient response of the closed loop adaptive system, (*ii*) develop a framework for analysis of its performance and robustness characteristics, or (*iii*) provide systematic guidelines for its design. These are the critical barriers for certification of adaptive flight control systems mentioned earlier.

Motivated by Rohrs' counterexample, we extend in this paper the setup introduced in [4,5] to a flight

test environment, and then propose a methodology for validation of adaptive flight control systems. To make things more precise, the first order nominal stable plant used in Rohrs' simulations is replaced by a small unmanned aerial vehicle (UAV) controlled by a commercial autopilot (AP). This nominal plant, consisting of the closed loop UAV with its autopilot, is augmented with an adaptive controller for improved angular rate tracking capabilities in the presence of different artificially "injected" unmodeled dynamics. Then, this flight test setup is used to demonstrate the advantages of $\mathcal{L}_1$ adaptive control as a *verifiable* robust adaptive control architecture with the potential of reducing flight control design costs and facilitating the transition of adaptive control into advanced flight control systems of general aviation. The main benefit of $\mathcal{L}_1$ adaptive control is its *fast* and *robust* adaptation, which does not interact with the robustness characteristics of the closed loop adaptive system.[24] In fact, the architectures of $\mathcal{L}_1$ adaptive control theory have *guaranteed transient performance* and *guaranteed robustness* in the presence of *fast adaptation*, without introducing or enforcing persistence of excitation, without any gain scheduling of the controller parameters, and without resorting to high–gain feedback. In these architectures, the speed of adaptation is limited only by the available computational power and the noise introduced by sensors, while the trade off between performance and robustness can be resolved via conventional methods from classical and robust control. The philosophy of $\mathcal{L}_1$ adaptive control architectures is to obtain the estimate of the uncertainties via a fast estimation scheme and define the control signal as the output of a low pass linear filter which, not only guarantees that the control signal stays in the low frequency range in the presence of fast adaptation, but also leads to separation between adaptation and robustness; in fact, it defines the trade off between performance and robustness. In particular, proper filter design leads to desired transient performance for the system input and output signals simultaneously, in addition to steady state tracking.[25] It also has guaranteed, analytically provable, bounded away from zero time–delay margin.[26] Moreover, the systematic design procedures of the $\mathcal{L}_1$ adaptive control theory significantly reduce the tuning effort required to achieve desired closed loop performance. With these features, the $\mathcal{L}_1$ adaptive control architectures provide a suitable framework for development of theoretically justified tools for Verification and Validation of feedback systems, thus creating the opportunity to close some of the principal gaps in certification of adaptive flight control systems.

The novelty of this paper is twofold. First, it reports new results on the verification and in–flight validation of the recently developed $\mathcal{L}_1$ adaptive flight control system; and second, it proposes a general methodology for safe verification and validation of adaptive flight control systems. The suggested framework, which is inspired by Rohrs' counterexample, allows for verification of the theoretical claims of $\mathcal{L}_1$ adaptive control, and for assessment of the performance and robustness characteristics of the inner loop $\mathcal{L}_1$ adaptive flight control system currently tested at the Naval Postgraduate School. The framework can also be used for verification and validation of other adaptive control algorithms, and hence explicitly addresses one of the main goals of the IRAC program.

The paper is organized as follows. Section II presents the flight test setup adopted for in–flight validation of adaptive flight control systems and introduces some tools used to evaluate performance of the closed loop adaptive system. Section III addresses the identification of the frequency response of the nominal plant consisting of the UAV with its autopilot, and presents the two output feedback adaptive algorithms tested in flight. Hardware–in–the–Loop (HIL) experiments are used to tune these adaptive algorithms to achieve desired performance and robustness characteristics. Section IV extends Rohrs' counterexample to the flight test environment and describes the results obtained in HIL simulations and flight tests. In particular, three experiments are reported. The first experiment considers the case of artificially injected unmodeled dynamics, introducing uncertainty both at high frequencies and inside the bandwidth of the UAV dynamics. In the second experiment, a second order model, simulating the effects of flexible aircraft dynamics, is injected at the output of the plant. The third experiment illustrates the capabilities of the adaptive algorithms when recovering from a sudden control surface failure. Finally, Section V summarizes the key results and contains the main conclusions.

II. Preliminaries of the Study

A. Rapid Flight Test Prototyping System

Recognizing the value of experimental V&V of advanced flight control algorithms, the Naval Postgraduate School (NPS) team has developed the so–called Rapid Flight Test Prototyping System (RFTPS).[27] The RFTPS consists of a testbed UAV equipped with a commercial autopilot, an embedded computer running the research algorithms in real time, and a ground control station for flight management and data moni-

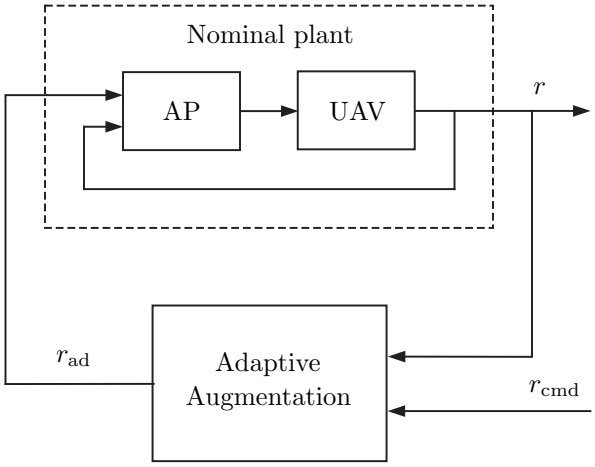

Figure 1: Inner loop adaptive augmentation loop tested by NPS

toring/collection. This system facilitates the real time onboard integration of advanced control algorithms, and provides the opportunity to design and conduct comprehensive flight test programs to evaluate the robustness and performance characteristics of these algorithms.

In order to demonstrate the benefits of $\mathcal{L}_1$ adaptive control, the commercial autopilot of the RFTPS has been augmented with the $\mathcal{L}_1$ adaptive output feedback architectures presented in [28] and [29]. The $\mathcal{L}_1$ augmentation loop is introduced to enhance the turn rate tracking capabilities of the autopilot in the event of control surface failures and in the presence of significant environmental disturbances. The inner loop adaptive flight control architecture implemented on the RFTPS is represented in Figure 1. Preliminary flight test results of this setup were first reported in [30], where the authors analyzed stability and performance of the $\mathcal{L}_1$ adaptive control system in the presence of locked–in–place control surface failures. The results obtained demonstrated that the $\mathcal{L}_1$ augmented system provides fast recovery to sudden failures in either one of the ailerons or in the rudder, while the unaugmented system would go unstable.

In the present paper, the RFTPS is modified to permit an "artificial injection" of unmodeled dynamics at the output of the closed loop UAV and autopilot system (see Figure 2). This setup, which is inspired by Rohrs' counterexample, provides an opportunity to evaluate the robustness and performance characteristics of adaptive flight control systems in the presence of different system uncertainties and output disturbances. In particular, for the purpose of this study, three cases of unmodeled dynamics are considered. In the first case, a second order transfer function introducing uncertainty both at high frequencies and inside the bandwidth of the UAV dynamics is injected. In the second case, we consider a very lightly damped second order transfer function introducing uncertainty well beyond the bandwidth of the (rigid) UAV, as an attempt to replicate the effects of flexible body modes. This second setup, hence, allows for identification of possible structural mode interactions between the UAV and the adaptive augmentation loop implemented onboard. Finally, the third scenario considers the injection of a locked–in–place control surface failure in the left aileron.

To verify that this setup replicates the phenomena observed in Rohrs' simulations and that it appropriately reflects the undesirable and unpredictable interactions between the adaptation process and the closed loop system dynamics, we first augment the onboard autopilot with a model reference adaptive control (MRAC) algorithm with similar robustness properties as the adaptive algorithm considered by Rohrs and coauthors. In addition, we also implement some of the modifications developed to overcome the problem of parameter drift in conventional MRAC, and demonstrate that in fact these modifications recover stability of the closed loop adaptive system. We emphasize that the objective of these preliminary experiments is only to calibrate the flight test setup and to verify correctness of the proposed framework. The flight test setup is then used to evaluate the stability, performance, and robustness properties of the $\mathcal{L}_1$ adaptive controller, and to verify the theoretical claims for $\mathcal{L}_1$ adaptive control architectures.

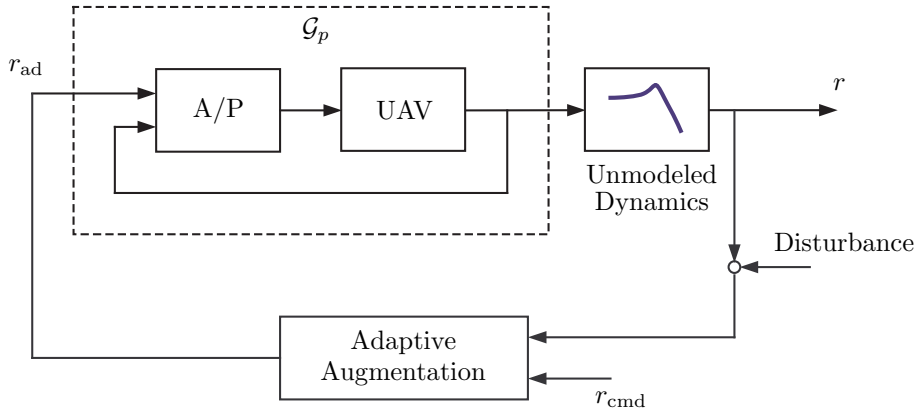

Figure 2: Closed loop adaptive system with artificially injected unmodeled dynamics and output disturbances

B. Bowditch–Lissajous Curves

To replicate Rohrs' simulations with the flight test setup introduced above, we first need to determine the frequency response of the nominal plant consisting of the UAV and its autopilot. To this end, we exploit the properties and benefits of the *Bowditch–Lissajous curves*. This family of curves is named after two scientists: the American mathematician Nathaniel Bowditch, who studied them in 1815; and the French mathematician Jules Antoine Lissajous, who independently studied these curves in more detail in 1857. A Bowditch–Lissajous curve is a curve described by the equations

$$x(t) = A\sin(\omega_x t - \phi_x) \quad (1)$$
$$y(t) = B\sin(\omega_y t - \phi_y)\,, \quad (2)$$

which are parameterized by the amplitudes A and B, the frequencies ω_x and ω_y, and the phase shifts ϕ_x and ϕ_y. The shape of this two–dimensional curve is a function of its parameters, and in particular it is closed if and only if the ratio $\frac{\omega_x}{\omega_y}$ is rational. More details on Bowditch–Lissajous curves can be found in [31].

It is well known that, when a linear–time–invariant (LTI) system is driven by a sinusoidal input signal, its output response is also a sinusoidal signal at the same frequency but with different amplitude and phase shift, the last two being functions of the frequency of the input signal. Then, the curve generated by plotting the output of the LTI system against its input is an ellipse, which is a Lissajous curve for the special case of $\omega_x = \omega_y$. The *eccentricity* of the Lissajous curve is related to the phase shift between input and output, while the ratio of the projections of its body onto the y– and x–axes defines the magnitude of the frequency response.

These properties of the Lissajous curves are exploited in this paper for determination of the frequency response of the closed loop UAV with its autopilot, while being operated in its linear range. In addition, the Lissajous curves appeared to be a very useful tool to evaluate performance of adaptive flight control systems. In fact, the Lissajous curve generated by plotting the output response signal of the actual closed loop adaptive system against the output response of the corresponding reference system can provide a quantitative and accurate assessment of the performance of the adaptive control algorithm, eliminating any ambiguities in the noisy experimental data. Moreover, for the particular application considered in this paper, in which an inner loop autopilot is augmented with an adaptive controller, the Lissajous curve obtained by plotting the adaptive control signal (which is the command signal sent to the autopilot, see Figure 1) against the reference signal to be tracked offers very valuable information about the behavior of the adaptive controller. The quick and intuitive interpretation of Lissajous curves was particularly effective in monitoring the performance of the adaptive controllers during the flight test experiments in real time.

III. Frequency Response Analysis and Adaptive Augmentation Loop Design

A. Frequency Response Analysis of the Nominal Plant

As mentioned earlier, the extension of Rohrs' counterexample requires identification of the frequency response of the closed loop UAV with its autopilot. This result will be useful later in the paper to determine the phase crossover frequency of the system with the artificially injected uncertainties, which is a necessary step to reproduce Rohrs' results. At the same time, having a (linear) model of the nominal plant is also important for the design of the adaptive augmentation loops, as the architecture of adaptive output feedback schemes usually depends on the structure of the plant to be controlled.

To determine the frequency response of the nominal plant, a sinusoidal signal was sent as a turn rate command to the autopilot. In particular, this reference signal was of the form

$$r_{\text{cmd}}(t) = A\sin(\omega t)$$

with tunable A–amplitude and ω–frequency. A set of Lissajous curves for the turn rate response of the closed loop UAV with the autopilot, together with their filtered least mean square estimates (in red), is presented in Figure 3. Table 1 summarizes the frequency response results derived from the Lissajous curves estimates. These results correspond to HIL simulations.

An analysis of the frequency response results of the nominal system and previous system identification work on the Rascal UAV (see [30]) shows that the turn rate response of the nominal plant can be modeled in the linear range as the following second order transfer function:

$$G_p(s) \approx \frac{\frac{1}{0.5}s + 1}{\frac{1}{0.55^2}s^2 + \frac{2\cdot 0.8}{0.55}s + 1},$$

which has a relative degree $n^* = 1$.

B. Adaptive Augmentation Algorithms

In this paper, the autopilot mounted onboard the UAV is augmented with an adaptive output feedback controller that modifies the turn–rate reference signal based on actual turn–rate measurements and sends the augmented command to the autopilot. As explained earlier, the main objective of wrapping an adaptive augmentation around the autopilot is to analyze whether turn–rate tracking performance and aircraft safety in the event of control surface failures and vehicle damage can be improved.

In this section, we present different adaptive algorithms that have been implemented onboard the RFTPS and tested both in hardware–in–the–loop simulations and in in–flight experiments. First, we introduce a conventional output feedback MRAC algorithm with properties similar to the adaptive controller used in [5]. In addition, we introduce some of the adaptive law modifications developed over the years to overcome the problem of parameter drift in conventional MRAC. These adaptive algorithms, with and without modifications, are used to check the validity of the flight test setup and to verify that the phenomena observed in Rohrs' simulations can be replicated. Finally, we also present the $\mathcal{L}_1$ adaptive output feedback control architecture implemented on the RFTPS, which has been proven to enhance the angular rate tracking capabilities of commercial off–the–shelf autopilots.[30,32]

1. MRAC Augmentation Algorithm

Several MRAC algorithms are available in the literature with similar robustness properties as the controller used in [5]. References [33] and [34] provide a good overview of this class of adaptive controllers. For the purpose of this paper, we use the algortihm presented in [34, Section 6.4]. The structure of this controller and some of the assumptions that need to be verified are introduced next. The reader is referred to [34] for more details on this algorithm. Next, we provide details on the implementation of the algorithm for the particular application at hand, and show HIL simulation results to demonstrate its performance capabilities.

Direct MRAC with Unnormalized Adaptive Laws. This algorithm assumes a single–input single–output (SISO) plant of the following form:

$$G_p(s) = k_p\frac{Z_p(s)}{R_p(s)},$$

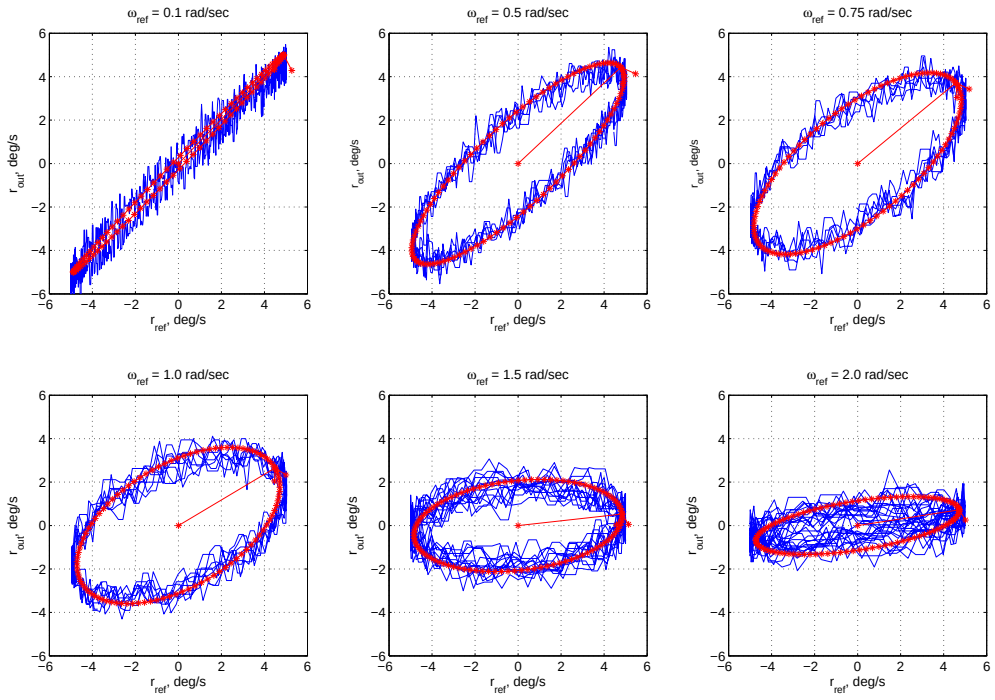

Figure 3: Lissajous curves $r(r_{\rm cmd})$ of the nominal plant for different frequencies.

Table 1: Frequency response of the closed loop UAV with its autopilot

Frequency, rad/s	0.1	0.5	0.75	1.0	1.5	2.0
Gain, dB	0.1	−0.4	−0.63	−2.5	−2.9	−6.8
Phase, deg	−5.4	−33.1	−45.85	−54.4	−78.7	−78.9

where $Z_p(s)$ and $R_p(s)$ are unknown monic polynomials, and thus k_p represents the unknown high frequency gain. The plant is assumed to be minimum–phase, while an upper bound n on the number of poles, the relative degree of the plant n^*, and the sign of the high frequency gain are assumed to be known.

The reference model that describes the desired dynamics is given by:

$$G_m(s) \quad = \quad k_m \frac{Z_m(s)}{R_m(s)}\,,$$

where $Z_m(s)$ and $R_m(s)$ are monic Hurwitz polynomials, while k_m is a constant. The reference model $G_m(s)$ is assumed to be SPR and with the same relative degree n^* as the plant $G_p(s)$.

The control law $u(t)$ that solves the model reference problem can be formulated using the following state–space realization:

$$\begin{aligned} \dot{\omega}_1(t) &= F\omega_1(t) + gu(t)\,, \quad \omega_1(0) = 0 \\ \dot{\omega}_2(t) &= F\omega_2(t) + gy(t)\,, \quad \omega_2(0) = 0 \\ u(t) &= \theta^\top(t)\omega(t)\,, \end{aligned} \tag{3}$$

where the Hurwitz matrix $F \in \mathbb{R}^{(n-1)\times(n-1)}$ and the vector $g \in \mathbb{R}^{n-1}$ are degrees of freedom available to the controller designer, $\omega_1(t), \omega_2(t) \in \mathbb{R}^{n-1}$ are internal regression signals, and $\theta(t) \in \mathbb{R}^{2n}$ is the vector of

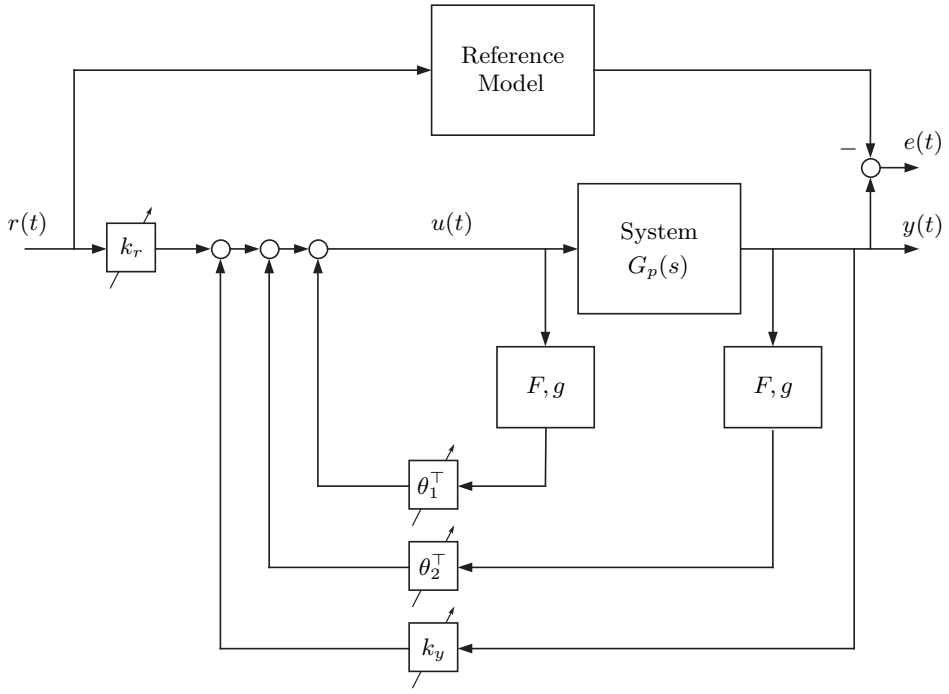

Figure 4: MRAC augmentation loop.

parameter estimates. Let $\omega(t) \in \mathbb{R}^{2n}$ be given by

$$\omega(t) \quad = \quad \left[\begin{array}{cccc} \omega_1^\top(t) & \omega_2^\top(t) & y(t) & r(t) \end{array} \right]^\top ,$$

where $y(t)$ and $r(t)$ represent the output of the plant and the reference signal respectively. Then the adaptation law for $\theta(t)$ is given by

$$\dot{\theta}(t) \quad = \quad -\Gamma e(t)\omega(t)\mathrm{sgn}\left(\frac{k_m}{k_p}\right) , \qquad \theta(0) = \theta_0 , \tag{4}$$

where $\Gamma > 0$ and $e(t) = y(t) - y_m(t)$, $y_m(t)$ is the output of the reference model $G_m(s)$ to the reference signal $r(t)$. The block diagram for this MRAC algorithm is presented in Figure 4. For details on the choice of the controller parameters F, g, and Γ, the reader is again referred to [34].

This formulation of the MRAC algorithm guarantees that:

1. all signals of the closed loop adaptive system are bounded and the tracking error $e(t)$ converges to zero asymptotically for any bounded reference signal $r(t)$.

2. if the reference signal $r(t)$ is sufficiently rich, $\dot{r}(t)$ is bounded, and the polynomials $Z_p(s)$ and $R_p(s)$ are relatively coprime, then the parameter error and the tracking error converge to zero exponentially fast.

To improve robustness properties of this algorithm, we consider the following modifications of the MRAC adaptive control law:

- **Projection operator:**

$$\dot{\theta}(t) \quad = \quad \Gamma \ \mathrm{Proj}\left(\theta(t), \ -e(t)\omega(t)\mathrm{sgn}\left(\frac{k_m}{k_p}\right)\right) , \qquad \theta(0) = \theta_0 ,$$

  where Proj represents the projection operator[35] defined over a given compact set Θ.

- σ–**modification:**

$$\dot{\theta}(t) \quad = \quad -\Gamma e(t)\omega(t)\text{sgn}\left(\frac{k_m}{k_p}\right) - \sigma\theta(t)\,, \qquad \theta(0) = \theta_0\,,$$

  where σ is a tunable positive parameter.

- e–**modification:**

$$\dot{\theta}(t) \quad = \quad -\Gamma e(t)\omega(t)\text{sgn}\left(\frac{k_m}{k_p}\right) - \gamma\theta(t)|e(t)|\,, \qquad \theta(0) = \theta_0\,,$$

  where γ is a tunable positive parameter.

MRAC Augmentation Loop Design. As shown in Section III.A, the closed loop UAV with the autopilot can be modeled in the low frequency range as a second order model of relative degree $n^* = 1$. Then, according to the design constraints of the MRAC algorithm presented above, we can choose the reference model to be a stable first order system of the form:

$$G_m(s) \quad = \quad \frac{m}{s+m}\,, \qquad m \;>\; 0\,,$$

which, at the same time, is an SPR transfer function. In fact, one can check that this reference model verifies all the assumptions stated in the description of the MRAC algorithm introduced in the previous section. The bandwidth of this reference model was chosen to be 1.5 $\frac{\text{rad}}{\text{s}}$, which is similar to the -3 dB bandwidth of the nominal airplane with the autopilot, as it can be seen in Table 1.

For the design of the MRAC algorithm, we will assume that the upper bound on the number of poles in the plant is $n = 2$. With this assumption, both $\omega_1(t)$ and $\omega_2(t)$ are just scalar signals, while the parameters F and g are scalar positive constants. Therefore, the vector $\omega(t)$ belongs to $\mathbb{R}^4$ and we will have a total of four adaptive parameters:

$$\theta(t) \quad = \quad \left[\begin{array}{cccc} \theta_1(t) & \theta_2(t) & k_y(t) & k_r(t) \end{array}\right]^\top\,,$$

where $\theta_1(t)$, $\theta_2(t)$, $k_y(t)$, and $k_r(t)$ are scalar parameters. The matrix of adaptive gains will be chosen to be a diagonal 4×4 matrix with positive entries.

The tunable parameters of the MRAC algorithm have been adjusted in HIL experiments with the objective of achieving a satisfactory convergence rate for the parameters without compromising the robustness of the closed loop adaptive system. The values of the parameters are given below:

$$\begin{aligned} F &= -2 \\ g &= 1 \\ \Gamma &= \text{diag}\left(\left[\begin{array}{cccc} 5 & 10 & 2 & 2.5 \end{array}\right]\right)\,, \end{aligned}$$

while the initial parameter estimate was set to

$$\theta_0 \quad = \quad \left[\begin{array}{cccc} 0 & 0 & 0 & 1 \end{array}\right]\,.$$

For this set of parameters, the time–delay margin (defined at the input of the system) obtained in simulation at the speed of 22 $\frac{\text{m}}{\text{s}}$ and altitude of 550 m is $\tau^* \approx 0.15$ s. We also emphasize here that the tuning of this MRAC algorithm has been done by trial–an–error, as there are no general systematic design guidelines for the design of this class of adaptive controllers.

Figure 5 shows the results of one of the experiments in the HIL environment. In particular, it shows the response of the closed loop adaptive system with the MRAC augmentation loop to a set of biased sinusoidal reference signals at different frequencies[a]. As one can see, the MRAC algorithm is able to asymptotically

[a]The reference signals used for the flight test experiments is of the form

$$r_{\text{cmd}}(t) = b \;+\; A\sin(\omega t)$$

with tunable b–bias, A–amplitude, and ω–frequency. Introducing a bias term b results in the airplane orbiting continuously in a bounded airspace box, which makes the flight experiment significantly easier to perform; the value of this bias term is chosen small enough to allow a reasonable flexibility in choosing the amplitude A without internally saturating the autopilot. For consistency, we also use biased sinusoidal reference signals in HIL simulations.

track the output of the reference system responding to the different sinusoidal reference signals. Figures 5a, 5d, and 5g demonstrate the adequacy of Lissajous curves, rather than time history plots, to assess closed loop performance for sinusoidal reference signals and, as we will see later in this paper, to analyze degradation in performance. It is important to note that, in the case of adaptive controllers in which the objective is to track the output of a reference system, the appropriate Lissajous curve to evaluate the closed loop performance is the one generated by plotting the output of the system, in this case the turn rate, against the output of the reference system used in the implementation of the adaptive controller. For sinusoidal reference signals, a Lissajous curve being a straight line of slope 1 would indicate that desired tracking performance is achieved. To illustrate this discussion, Figure 6 shows two different sets of Lissajous curves obtained from data from the previous experiment. Figure 6a is the result of overlapping the Lissajous curves presented in Figures 5a, 5d, and 5g. These three Lissajous curves are almost straight lines with slope 1, which indicates that the tracking objective of MRAC is (asymptotically) achieved. On the other hand, Figure 6b presents the Lissajous curves obtained by plotting the output of the system against the sinusoidal reference signal. Because the reference system introduces a phase shift to the reference signal, the eccentricity of the Lissajous curve decreases as the frequency of the reference signal increases.

Together with the tunable parameters of the MRAC algorithm, the different modifications of the adaptive laws were also adjusted in HIL. The objective was to improve the robustness of the standard MRAC algorithm without sacrificing significantly the performance of the closed loop adaptive system for reference signals in the low frequency range. The parameters chosen for the different modifications are detailed next:

- **Projection operator:** the bounds for the adaptive parameters were chosen as follows:

$$\theta_1(t), \theta_2(t), k_y(t) \in [-0.3,\ 0.3]\,, \quad \text{and} \quad k_r(t) \in [0.1,\ 2]\,.$$

- **σ-modification:** the value of the tunable parameter σ was chosen to be $\sigma = 0.075$.
- **e-modification:** the value of the tunable parameter γ was chosen to be $\gamma = 0.25$.

2. $\mathcal{L}_1$ Augmentation Algorithm

This section provides an overview of the $\mathcal{L}_1$ adaptive output feedback controller for systems of unknown dimension in the presence of unmodeled dynamics and time varying uncertainties. The reader is referred to [28] for a more detailed explanation of this architecture, as well as for the main results and their proofs. The section also includes HIL simulation results to illustrate the performance characteristics of this algorithm.

$\mathcal{L}_1$ Adaptive Output Feedback Controller for First Order Reference Systems. We start by considering the system

$$y(s) \;=\; G_p(s)\left(u(s) + z(s)\right)\,, \qquad y(0) = 0\,, \tag{5}$$

where $u(t) \in \mathbb{R}$ is the system's input, $y(t) \in \mathbb{R}$ is the system's output, $G_p(s)$ is assumed to be an unknown strictly proper transfer function, $z(s)$ is the Laplace transform of the time varying uncertainties and disturbances $d(t) = f(t, y(t))$, while $f : \mathbb{R}\times\mathbb{R} \to \mathbb{R}$ is an unknown map, subject to the following assumptions:

Assumption 1 *There exist constants $L > 0$ and $L_0 > 0$ such that the following inequalities*

$$\begin{aligned} |f(t, y_1) - f(t, y_2)| &\leq L\,|y_1 - y_2| \\ |f(t, y)| &\leq L|y| + L_0\,, \end{aligned}$$

hold uniformly in $t \geq 0$.

Assumption 2 *There exist constants $L_1 > 0$, $L_2 > 0$ and $L_3 > 0$ such that for all $t \geq 0$:*

$$|d(t)| \;\leq\; L_1|\dot{y}(t)| + L_2|y(t)| + L_3\,.$$

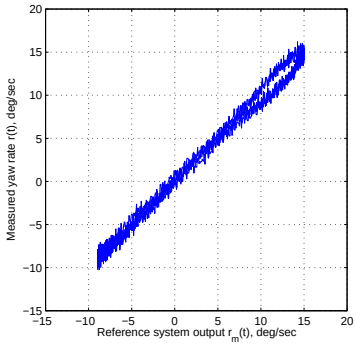

(a) Lissajous $r(r_m)$

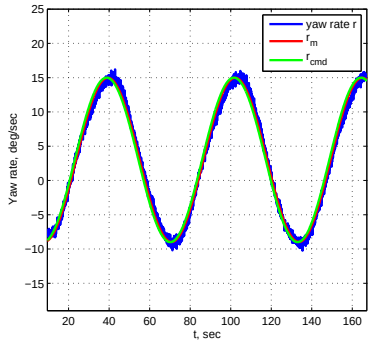

(b) Tracking performance

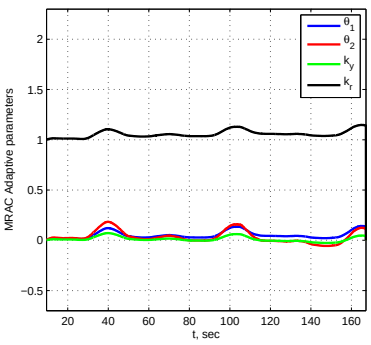

(c) MRAC parameters

Figure 5: MRAC. Closed loop response to a biased sinusoidal reference signal at $\omega = 0.1$ $\frac{\text{rad}}{\text{s}}$.

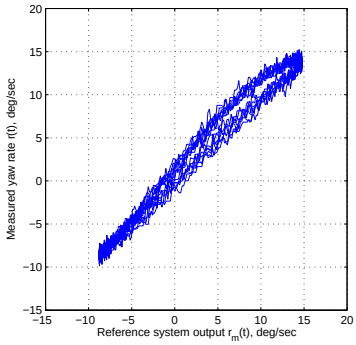

(d) Lissajous $r(r_m)$

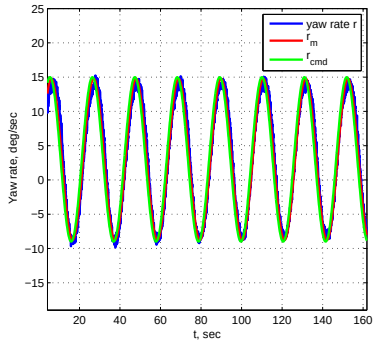

(e) Tracking performance

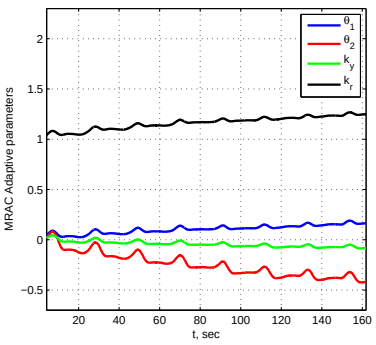

(f) MRAC parameters

Figure 5: MRAC. Closed loop response to a biased sinusoidal reference signal at $\omega = 0.3$ $\frac{\text{rad}}{\text{s}}$.

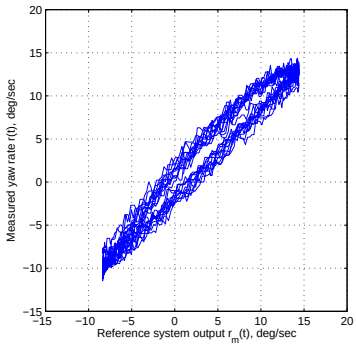

(g) Lissajous $r(r_m)$

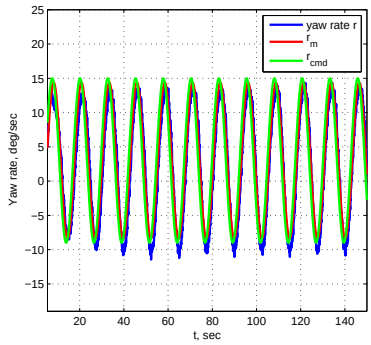

(h) Tracking performance

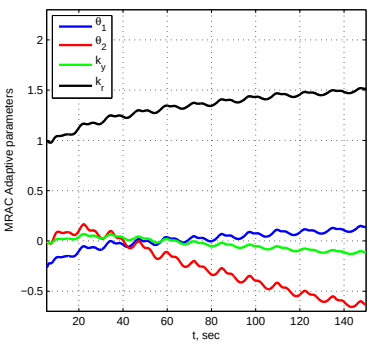

(i) MRAC parameters

Figure 5: MRAC. Closed loop response to a biased sinusoidal reference signal at $\omega = 0.5$ $\frac{\text{rad}}{\text{s}}$.

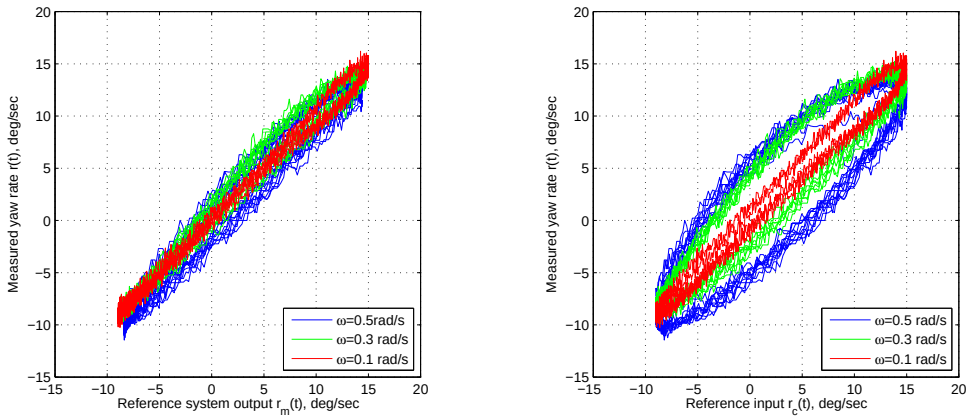

(a) Lissajous $r(r_m)$ (b) Lissajous $r(r_{\rm cmd})$

Figure 6: MRAC. Lissajous curves for the response of the closed loop system to biased sinusoidal reference signals at different frequencies.

We note that the numbers L, L_0, L_1, L_2, and L_3 can be arbitrarily large. The control objective is to design an adaptive output feedback controller $u(t)$ such that the system output $y(t)$ tracks the given bounded piecewise continuous reference signal $r(t)$ following a desired reference model $M(s)$. In this section, we consider a first order reference system, i.e.

$$M(s) = \frac{m}{s+m}\,, \qquad m > 0\,, \tag{6}$$

which is the same reference model that was implemented for the MRAC algorithm.

To provide an intuitive explanation behind the main idea of the $\mathcal{L}_1$ adaptive augmentation used in this paper, we note that the system in (5) can be rewritten in terms of the desired system $M(s)$ as

$$y(s) \;=\; M(s)\left(u(s)+\sigma(s)\right)\,, \qquad y(0)=0\,, \tag{7}$$

where the uncertainties due to $G_p(s)$ and $z(s)$ are lumped into the signal $\sigma(s)$, which is defined as

$$\sigma(s) \;=\; \frac{\left(G_p(s)-M(s)\right)u(s)+G_p(s)z(s)}{M(s)}\,. \tag{8}$$

The philosophy of the $\mathcal{L}_1$ adaptive output feedback controller is to obtain an estimate of the uncertain signal $\sigma(t)$, and define a *control signal* that compensates for the effects of this uncertainty within the bandwidth of a low pass filter $C(s)$ introduced in the control channel. This filter, which represents the key difference between $\mathcal{L}_1$ adaptive control and conventional MRAC, guarantees that the output of the $\mathcal{L}_1$ adaptive controller stays in the low frequency range in the presence of fast adaptation and large reference inputs, leads to separation between adaptation and robustness, and defines the trade off between performance and robustness. *Adaptation* is based on the projection operator, ensuring boundedness of the adaptive parameters by definition,[35] and uses the output of an *output predictor* to update the estimate of the uncertainty $\hat{\sigma}(t)$. This output predictor is defined to have the structure of the system (7), using the estimate $\hat{\sigma}(t)$ instead of $\sigma(t)$ itself, which is unknown. The $\mathcal{L}_1$ adaptive control architecture is represented in Figure 7 and its elements are introduced below.

Output Predictor: We consider the following output–predictor

$$\dot{\hat{y}}(t) = -m\hat{y}(t) + m\left(u(t)+\hat{\sigma}(t)\right), \qquad \hat{y}(0)=0\,, \tag{9}$$

where $\hat{\sigma}(t)$ is the adaptive estimate.

Adaptation Law: The adaptation of $\hat{\sigma}(t)$ is defined as

$$\dot{\hat{\sigma}}(t) = \Gamma_c \mathrm{Proj}(\hat{\sigma}(t), -\tilde{y}(t)),\ \hat{\sigma}(0)=0, \tag{10}$$

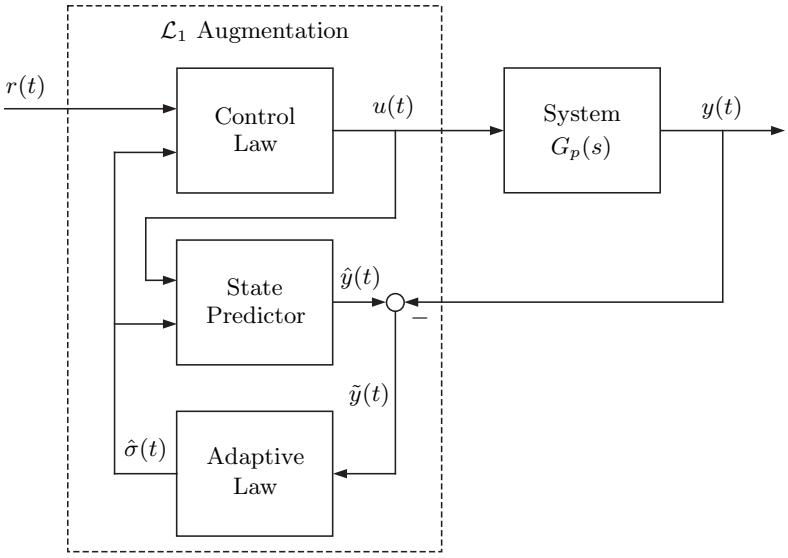

Figure 7: $\mathcal{L}_1$ adaptive augmentation loop.

where $\tilde{y}(t) = \hat{y}(t) - y(t)$ is the error signal between the output predictor in (9) and the output of the system in (5), $\Gamma_c > 0$ is the adaptation rate subject to a computable lower bound, and Proj denotes the projection operator.

Control Law: The control signal is generated by

$$u(s) \quad = \quad r(s) - C(s)\hat{\sigma}(s)\,, \tag{11}$$

where $C(s)$ is a strictly proper low pass filer with $C(0) = 1$.

The complete $\mathcal{L}_1$ adaptive output feedback controller consists of (9), (10) and (11) subject to the following stability condition: the design of $C(s)$ and $M(s)$ must ensure that

$$H(s) \quad = \quad \frac{G_p(s)M(s)}{C(s)G_p(s) + (1 - C(s))M(s)} \qquad \text{is stable,} \tag{12}$$

and in addition, the following $\mathcal{L}_1$–norm condition holds:

$$\|H(s)(1 - C(s))\|_{\mathcal{L}_1} L \quad < \quad 1\,. \tag{13}$$

Then, it has been proven that the control signal $u(t)$ and the output $y(t)$ of the closed loop adaptive system with the $\mathcal{L}_1$ adaptive controller in (9), (10), and (11) track both in *transient* and *steady state* the input and output of an auxiliary *closed loop reference system*, which is defined as the ideal nonadaptive version of the $\mathcal{L}_1$ adaptive controller assuming perfect knowledge of uncertainties. We refer to [28] for a detailed derivation of these proofs.

$\mathcal{L}_1$ Augmentation Loop Design. The $\mathcal{L}_1$ augmentation scheme is tuned to achieve a similar level of performance as the MRAC algorithm for reference signals in the low frequency range and, at the same time, have similar robustness characteristics. The reference model was chosen to be exactly the same as for the MRAC algorithm, that is, a stable first order system with bandwidth 1.5 $\frac{\text{rad}}{\text{s}}$. The adaptive gain was set to $30,000$, while the low pass filter was chosen to be a first order system with unity DC gain and 0.6 $\frac{\text{rad}}{\text{s}}$ of bandwidth. This choice for the low pass filter ensures a satisfactory level of performance with a time–delay margin (in simulation) of $\tau^* \approx 0.15$ s at the same flight condition of 22 $\frac{\text{m}}{\text{s}}$ and 550 m.

Figure 8 shows the results from one of the HIL experiments conducted to tune the $\mathcal{L}_1$ adaptive augmentation loop. In particular, it shows the response of the closed loop adaptive system with the $\mathcal{L}_1$ augmentation loop to a set of biased sinusoidal reference signals at different frequencies. The $\mathcal{L}_1$ adaptive is able to perfectly

track the output of the reference system to sinusoidal reference signals in the low frequency range (≤ 0.1 $\frac{\text{rad}}{\text{s}}$), as the Lissajous curve in Figure 8a illustrates. Moreover, one can observe in Figure 8c that the contribution of the $\mathcal{L}_1$ controller, $-C(s)\hat{\sigma}(s)$, to the reference signal r_{cmd} is almost zero during this experiment, and only becomes significant at high turn rates, which are characterized by high bank angle attitudes with nonlinear dynamics. This indicates that the autopilot mounted onboard the UAV is able to precisely track reference signals in the low frequency range and in the linear range of the UAV, while the adaptive controller helps the autopilot only when needed. Further, Figures 8d–8f and 8g–8i show that, as the frequency of the reference signal increases beyond the bandwidth of the low pass filter $C(s)$, the eccentricity of the Lissajous curves decreases, which reveals a degradation in tracking performance, consistent with the theory of $\mathcal{L}_1$ adaptive control.

IV. Rohrs' Counterexample in Flight

In this section we describe the results obtained both in HIL simulations and flight tests for the different experiments proposed in Section II. In particular, we first verify that the phenomena observed in Rohrs' simulations illustrating the limitations of conventional MRAC algorithms can be reproduced by the flight test setup proposed in this paper. We also verify that the adaptive law modifications introduced to improve the robustness of conventional MRAC algorithms solve, under appropriate tuning, the problem of parameter drift. Specifically, results are only shown for the e–modification, but similar results have been obtained for the MRAC algorithm with projection operator and with σ–modification. We emphasize again that the objective of these first preliminary steps in the experiments is only to verify correctness of the proposed framework. Finally, we analyze the stability and performance characteristics of the closed loop system with the $\mathcal{L}_1$ adaptive augmentation loop, and verify the theoretical claims of $\mathcal{L}_1$ adaptive control.

A. Hardware–in–the–Loop Simulations

1. Second Order Unmodeled Dynamics

In this section, we artificially introduce at the output of the nominal plant (closed loop UAV and AP) a second order system representing unmodeled dynamics, similar to Rohrs' counterexample. In his counterexample, Rohrs considered the case of very well damped unmodeled dynamics at high frequencies to show that, even in the presence of apparently "harmless" uncertainties, the stability of adaptive controllers was not guaranteed. In this paper, nevertheless, we consider the case of more challenging uncertainties, with the objective of evaluating the performance and robustness of the $\mathcal{L}_1$ adaptive augmentation in the presence of unmodeled dynamics. In particular, we choose a low damped second order system with natural frequency approximately equal to the bandwidth of the plant, i.e.

$$\Delta(s) \quad = \quad \frac{\omega_n^2}{s^2 + 2\zeta\omega_n s + \omega_n^2}\,,$$

with $\omega_n = 1.5$ $\frac{\text{rad}}{\text{s}}$ and $\zeta = 0.45$.

With the addition of this second order system, the new plant has the phase crossover frequency approximately at 1.6 $\frac{\text{rad}}{\text{s}}$. Figure 9 shows the Lissajous curve of the system output plotted against the reference signal for the cascaded system in response to the biased sinusoidal reference signal at 1.6 $\frac{\text{rad}}{\text{s}}$. As one can observe, the Lissajous curve exhibits a phase shift of -180 deg, which confirms that 1.6 $\frac{\text{rad}}{\text{s}}$ corresponds to the phase crossover frequency of the cascaded system.

At this point, having identified the phase crossover of the system, we can extend Rohrs' results to the flight test setup considered in this paper. To this end, we consider the MRAC algorithm described in Section III. Figure 10 shows the response of the plant with the artificially injected second order unmodeled dynamics to biased sinusoidal reference signals at different frequencies. The closed loop adaptive system is able to asymptotically track the output of the reference model for reference signals at in the low frequency range ($\omega = 0.1$ $\frac{\text{rad}}{\text{s}}$ and $\omega = 0.5$ $\frac{\text{rad}}{\text{s}}$). However, when the system is driven by a reference signal at $\omega = 1$ $\frac{\text{rad}}{\text{s}}$, *bursting* takes place ($t \in [330\,\text{s},\ 350\,\text{s}]$). During this interval of time, the MRAC algorithm generates adaptive command signals with amplitudes reaching ± 100 $\frac{\text{deg}}{\text{s}}$, and the turn–rate tracking performance becomes very poor. Note that, for safety reasons, the autopilot has internal saturations which limit the commands sent to the UAV; without these internal saturations, the UAV would probably have been lost. This temporary

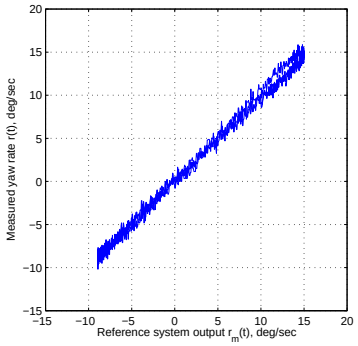

(a) Lissajous $r(r_m)$

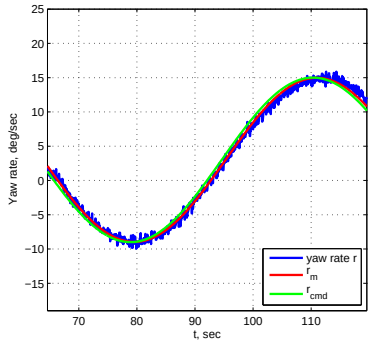

(b) Tracking performance

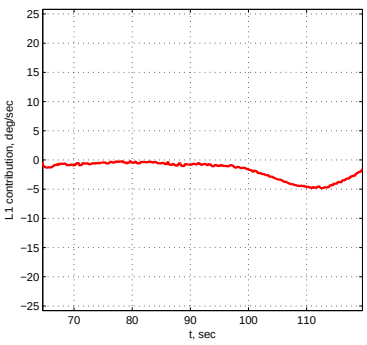

(c) $\mathcal{L}_1$ contribution

Figure 8: $\mathcal{L}_1$. Closed loop response to biased sinusoidal reference signal at $\omega = 0.1$ $\frac{\text{rad}}{\text{s}}$.

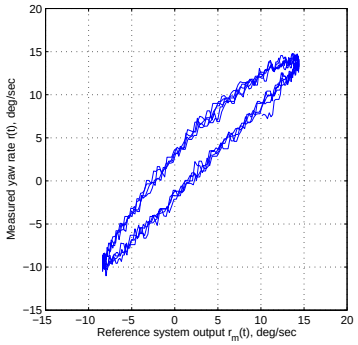

(d) Lissajous $r(r_m)$

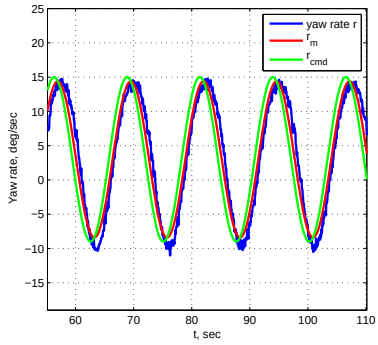

(e) Tracking performance

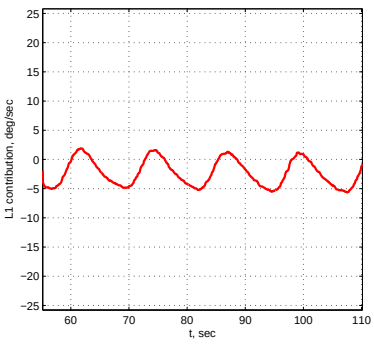

(f) $\mathcal{L}_1$ contribution

Figure 8: $\mathcal{L}_1$. Closed loop response to biased sinusoidal reference signal at $\omega = 0.5$ $\frac{\text{rad}}{\text{s}}$.

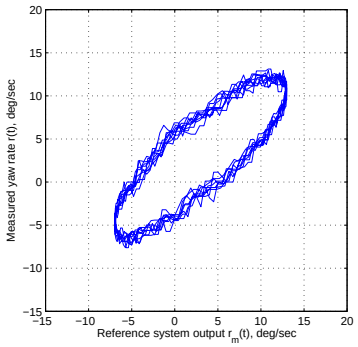

(g) Lissajous $r(r_m)$

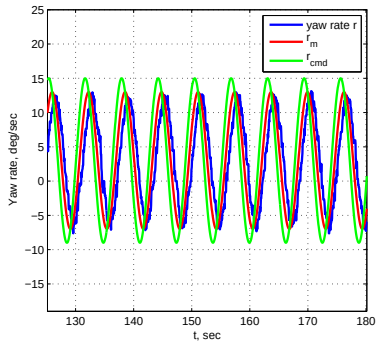

(h) Tracking performance

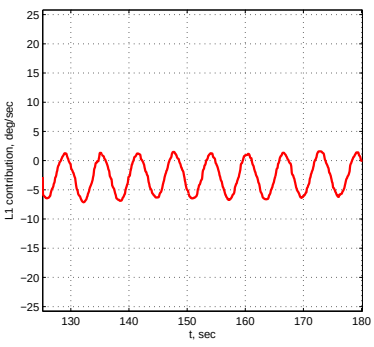

(i) $\mathcal{L}_1$ contribution

Figure 8: $\mathcal{L}_1$. Closed loop response to biased sinusoidal reference signal at $\omega = 1.0$ $\frac{\text{rad}}{\text{s}}$.

instability can be clearly observed in Figures 10a and 10c. Also, Figure 10d shows that there is an abrupt change in the adaptive parameter $\theta_1(t)$, which converges to a new value that stabilizes the system and achieves asymptotic tracking of the output of the reference model. Finally, when the system is driven by a reference signal at approximately the phase crossover frequency, $\omega = 1.6\ \frac{\text{rad}}{\text{s}}$, *parameter drift* takes place and the closed loop system with the MRAC algorithm becomes unstable.

These results are not new, and just replicate the well known limitations of conventional MRAC algorithms shown by Rohrs and coauthors in a flight test environment. As we previously mentioned, several modifications of the adaptive laws were developed during the last thirty years to improve robustness of MRAC architectures and solve the problem of parameter drift. Figure 11 shows the results of the same experiment obtained for the MRAC algorithm with the e–modification. It can be seen that the parameters stay bounded (Figure 11d) and the system remains stable for the whole experiment. However, as expected, significant degradation in tracking performance is observed. This degradation is evident in Figure 11a, which presents Lissajous curves far from the desired straight line with slope 1, thus indicating that the output of the plant barely tracks the output of the reference model even for reference signals in the low frequency range. It is important to note that further tuning of the MRAC algorithm and its modifications can be done, which might result in improved tracking performance. However, fine tuning will not change the nature of MRAC algorithms, for which there are no performance and robustness guarantees.

These experiments illustrate the lack of predictability of conventional MRAC algorithms, a fundamental limitation for certification of adaptive flight control systems. The degradation of performance resulting from the implementation of damping type modifications in the adaptive laws has also been shown. These results confirm that the proposed flight test setup is able to replicate the adverse interactions between the adaptation process and the closed loop system dynamics, verifying correctness of the framework developed in this paper.

Next we present the results obtained for the same experiment with the $\mathcal{L}_1$ adaptive augmentation (Figure 12). As it can be seen, the closed loop adaptive system is able to track precisely the output of the reference system to the reference signal at $\omega = 0.1\ \frac{\text{rad}}{\text{s}}$. As the frequency of the reference signal increases and goes beyond the bandwidth of the low pass filter $C(s)$, the tracking performance degrades as expected. Figure 12a illustrates the consistency in the response of the closed loop adaptive system, which traces very neat trajectories in the Lissajous plot. Moreover, Figure 12d shows that the contribution of the $\mathcal{L}_1$ adaptive controller does not exhibit high frequency content and remains within reasonable bounds, well inside the projection bounds for the (only) adaptive parameter $\hat{\sigma}(t)$. We emphasize that fast adaptation is the key for consistent input and output system response with desired performance in the low frequency range, while the low pass filter guarantees a desired level of robustness in the presence of this fast adaptation. The ability to adapt fast without sacrificing robustness of the closed loop adaptive system is the main difference between $\mathcal{L}_1$ adaptive control and MRAC with or without its adaptive law modifications.

2. Structural Mode Interactions

In this section we extend the philosophy of the previous experiment to the case of high frequency unmodeled dynamics with very low damping. This experiment has as a goal to reproduce the effects of bending modes in an airplane, and investigate the possible interaction between adaptive control and aircraft flexible dynamics. To this end, we choose a very low damped second order transfer function with natural frequency equal to approximately 7 times the bandwidth of the plant, i.e.

$$\Delta(s) \quad = \quad \frac{\omega_n^2}{s^2 + 2\zeta\omega_n s + \omega_n^2}\,,$$

with $\omega_n = 10\ \frac{\text{rad}}{\text{s}}$ and $\zeta = 0.01$, and at the same time we introduce a perturbation in the feedback signal at exactly $\omega = 10\ \frac{\text{rad}}{\text{s}}$:

$$d(t) \quad = \quad 20\sin(10t)\ \frac{\text{deg}}{\text{s}}\,.$$

Figure 13 shows the response of the system with the conventional MRAC algorithm to a biased sinusoidal reference signal at $\omega = 0.5\ \frac{\text{rad}}{\text{s}}$. Initially, we wait for the MRAC parameters to converge, so that the output of the system tracks the output of the reference model. At $t = 50$ s, the dynamics representing the bending mode are "injected", and the system runs in this configuration for approximately 30 s. The "injection" of

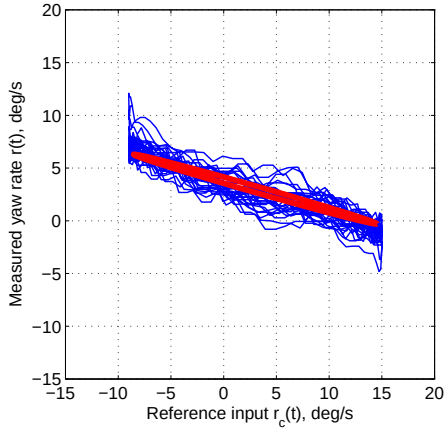

Figure 9: Lissajous curve for the nominal system with unmodeled dynamics driven by a biased sinusoidal reference signal at the phase crossover frequency ($\omega = 1.6\ \frac{\text{rad}}{\text{s}}$).

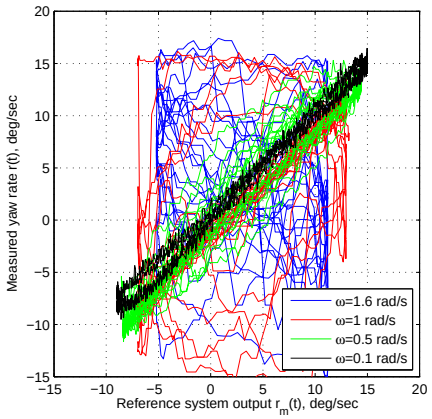

(a) Lissajous $r(r_m)$

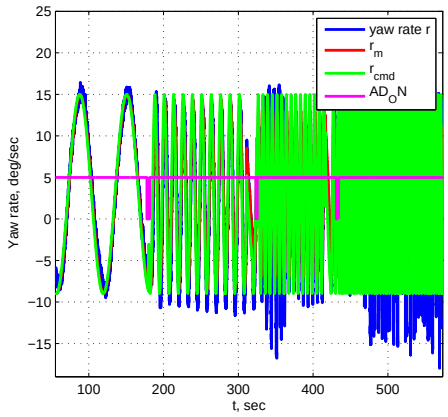

(b) Tracking performance

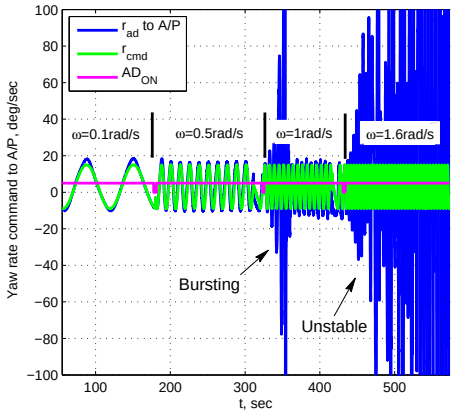

(c) Adaptive command to AP

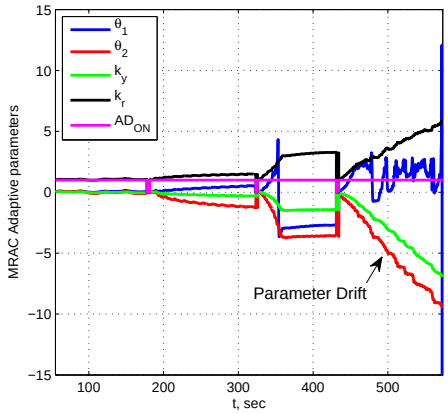

(d) MRAC parameters

Figure 10: MRAC. Closed loop response in the presence of second order unmodeled dynamics to biased sinusoidal reference signals at different frequencies.

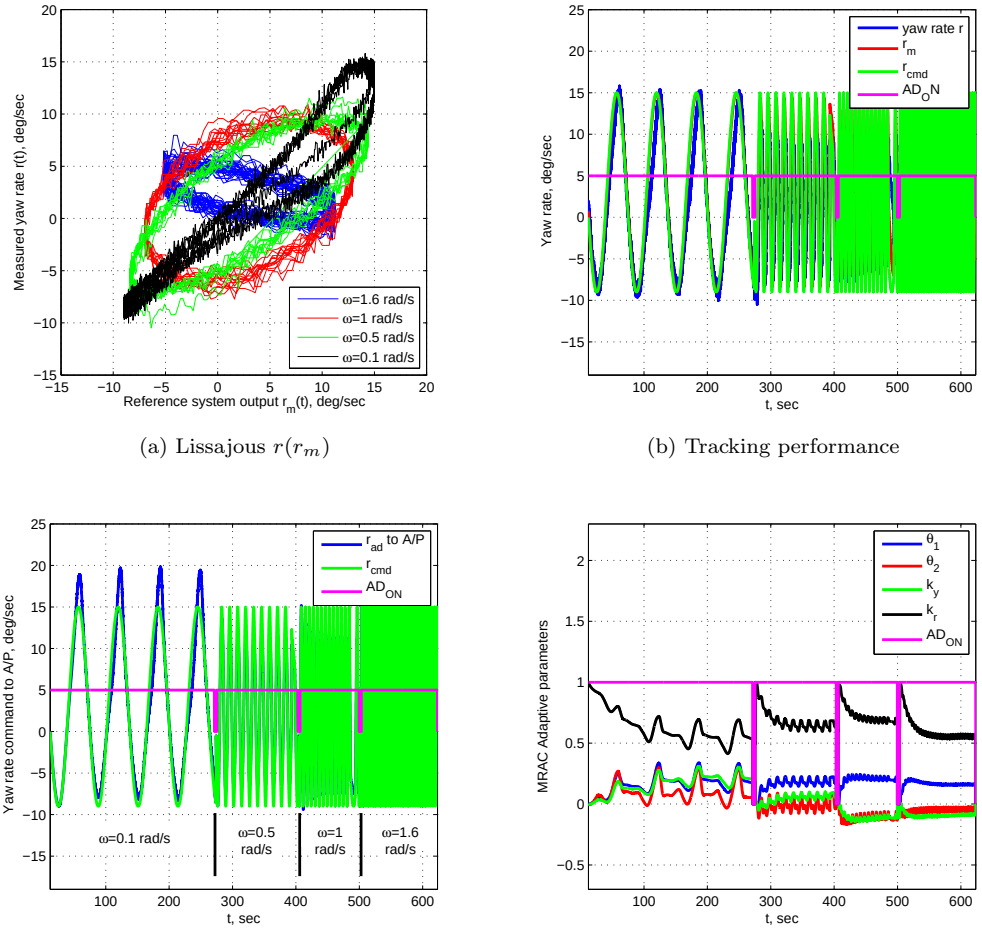

(a) Lissajous $r(r_m)$

(b) Tracking performance

(c) Adaptive command to AP

(d) MRAC parameters

Figure 11: MRAC with e–modification. Closed loop response in the presence of second order unmodeled dynamics to biased sinusoidal reference signals at different frequencies.

the bending mode introduces very small oscillations at the output of the plant, probably due to the presence of noise. We can see that initially the adaptive parameter $k_y(t)$ is close to zero, which implies that these oscillations at the output of the plant are well attenuated inside the adaptive controller and do not propagate to the control signal that the MRAC augmentation loop sends to the autopilot. Therefore, the bending mode is not excited and, during these 30 s, the MRAC algorithm is able to track the output of the reference model without exciting the bending mode. At approximately $t = 120$ s, we inject the disturbance in the feedback signal. One can see that there is a 10 s transient phase with high frequency oscillations at the output of the plant. These initial oscillations damp down and MRAC recovers a similar level of performance as the one before the injection of the disturbance. A similar result is obtained when the disturbance is disabled at $t = 180$ s. However, when we inject the disturbance for a second time at $t = 200$ s, the adaptive parameters start drifting immediately. In particular, we see that the parameter $k_y(t)$ grows significantly fast, which implies that the high frequency content at the output of the plant is amplified by the MRAC algorithm and sent to the autopilot, resulting in an unstable closed loop adaptive system. This experiment illustrates that conventional MRAC is not able to cope with lightly damped high frequency unmodeled dynamics, as it generates a counteracting control signal that tries to cancel the disturbances by "fighting" the attenuating capabilities of the autopilot. The result is an unstable closed loop system that increasingly excites the bending mode.

When the MRAC algorithm is implemented with the e–modification, the system retains stability along the whole experiment, Figure 14. Nevertheless, the slow adaptation in the parameters due to a deficient

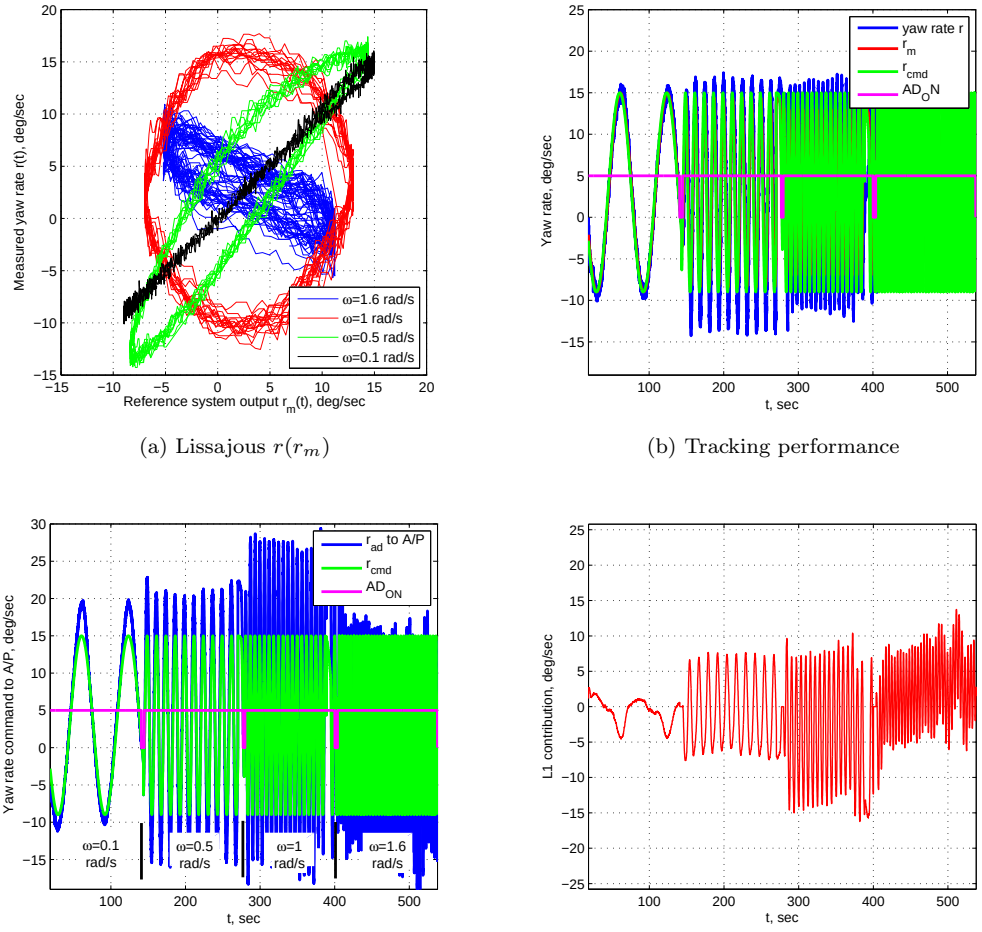

(a) Lissajous $r(r_m)$

(b) Tracking performance

(c) Adaptive command to AP

(d) $\mathcal{L}_1$ contribution

Figure 12: $\mathcal{L}_1$. Closed loop response in the presence of second order unmodeled dynamics to biased sinusoidal reference signals.

adaptive law results in poor high frequency disturbance attenuation characteristics. The time segments $t = [80,\ 150]$ s and $t = [150,\ 220]$ s explicitly illustrate this phenomenon: as the bending mode and the disturbance are "injected", the adaptive parameter $k_y(t)$ abruptly changes in an attempt to cancel the disturbance artificially injected in the feedback signal. As a result, this high frequency disturbance is not sufficiently attenuated inside the adaptive augmentation loop, which leads to significant oscillations at the output of the plant.

Next, Figure 15 presents the results obtained with the $\mathcal{L}_1$ adaptive controller. At $t = 50$ s the bending mode is "injected", which —similar to MRAC— results in very small amplitude oscillations at the output of the system due to the presence of noise. During this initial phase, the contribution of the $\mathcal{L}_1$ adaptive controller stays in the low frequency range. The disturbance is "injected" at $t = 108$ s. One can see that the $\mathcal{L}_1$ adaptive controller generates small oscillations in the control channel, which causes a 5 s transient at the output of the system with oscillations of approximately 1.5 Hz. These oscillations in the contribution of the $\mathcal{L}_1$ adaptive controller are due to the fact that the projection bounds in the adaptive law are too tight to handle the initial transient produced by the disturbance. Figure 16 shows that the uncertainty estimate $\hat{\sigma}(t)$ hits the bounds of projection, and as a consequence, the error between the output of the predictor $\hat{r}(t)$ is not able to track the output of the actual turn rate $r(t)$. These oscillations could be easily avoided by increasing the bounds of the projection operator and, if necessary, increasing the adaptation gain to reduce the tracking error between the output of the predictor and the output of the plant. In the experiment, after these 5 s of transient, the oscillations damp down and the $\mathcal{L}_1$ adaptive controller recovers its initial

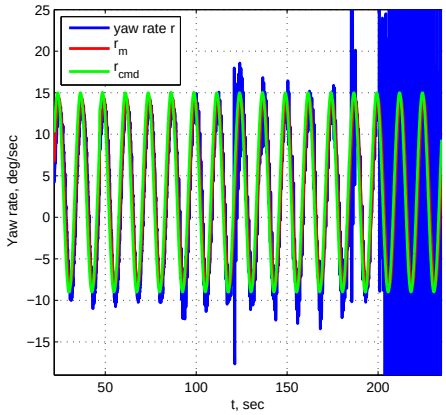

(a) Tracking performance

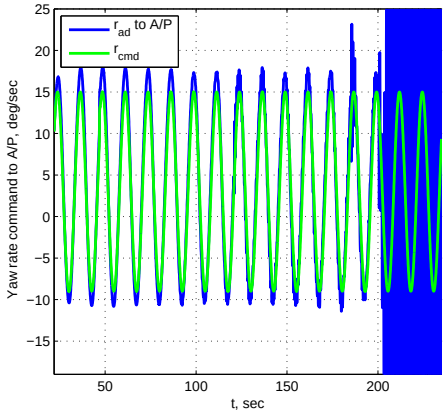

(b) Adaptive command to AP

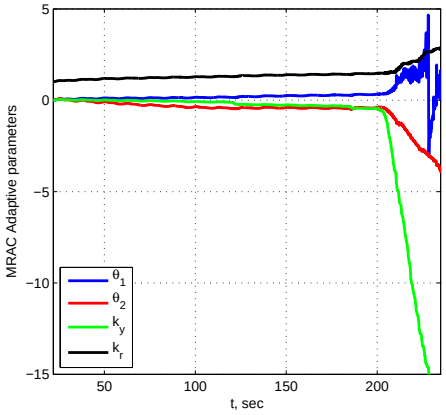

(c) MRAC parameters

Figure 13: MRAC. Closed loop response in the presence of bending modes to a biased sinusoidal reference signal at $\omega = 0.5 \ \frac{\text{rad}}{\text{s}}$.

performance. The presence of the low pass filter is critical in attenuating the high frequency content in the feedback signal and guaranteeing that the $\mathcal{L}_1$ contribution is within the low frequency range. The attenuating capabilities of the $\mathcal{L}_1$ controller do not lead to an adverse interaction with the autopilot, which is in contrast to the two MRAC algorithms presented above. In particular, this experiment shows that, if properly tuned, the $\mathcal{L}_1$ adaptive controller guarantees that its contribution is in the low frequency range and preserves the attenuating properties of the nominal inner loop, and thus the bending mode is not excited.

3. Control Surface Failures

In this section, instead of artificially introducing unmodeled dynamics at the output of the plant, we will consider the case of a sudden control surface failure affecting the nominal plant. In particular, the left aileron will get locked at -6 deg and then, after some time, we will recover full lateral control. This experiment is directly in line with the objectives of the IRAC–1.5.

First we show that the nominal plant with the autopilot is able to recover from the failure and track the reference signal with the remaining control authority[a]. Figure 17 shows the response of the plant to a biased sinusoidal reference signal at $\omega = 0.5 \ \frac{\text{rad}}{\text{s}}$. The failure is "injected" at $t = 375$ s, and the autopilot takes around 20 s to recover from the failure, which is the time that the integrators of the autopilot need to

[a]In [30], the autopilot was intentionally (de)tuned to demonstrate performance recovery capabilities of the $\mathcal{L}_1$ adaptive controller.

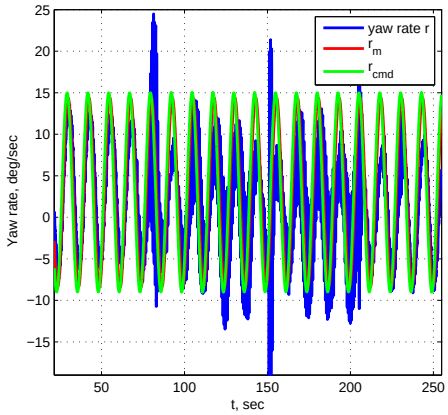

(a) Tracking performance

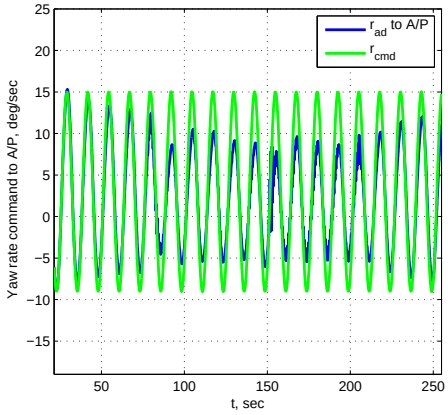

(b) Adaptive command to AP

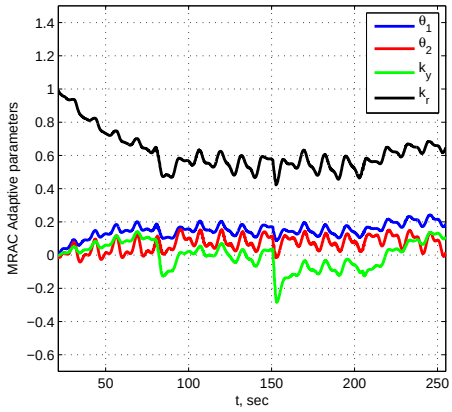

(c) MRAC parameters

Figure 14: MRAC with e–modification. Closed loop response in the presence of bending modes to a biased sinusoidal reference signal at $\omega = 0.5\ \frac{\text{rad}}{\text{s}}$.

readjust their contribution. The Lissajous curve shows that, in the presence of the failure, the autopilot is able to recover almost full performance with respect to the "healthy" UAV.

Next, we consider the case of the conventional MRAC algorithm. Figure 18 shows the response of the closed loop adaptive system. In the figure, one can see that initially the MRAC algorithm is able to track perfectly the output of the reference system. When the failure is introduced at $t = 190$ s, the MRAC algorithm is able to recover full performance in around 20 s and keep tracking the output of the reference system perfectly using the remaining control authority. The transient response is smooth and, as the integrators of the autopilot readjust, the command from the adaptive augmentation loop to the autopilot converges to the nominal adaptive contribution for the healthy UAV. However, when the UAV recovers full control authority ($t = 290$ s), the adaptive parameters drift and the closed loop system with the MRAC algorithm becomes unstable. For the sake of clarity, we did not add to the Lissajous curve the third phase in which the UAV recovers full lateral control authority and the system becomes unstable.

Again, this result is not new. The only objective of this experiment is to verify that the same instability results could be obtained in the event of a control surface failure. Figure 19 shows that parameter drift can be avoided with the introduction of the e–modification at the price of degraded performance. In this experiment, the aileron failure is introduced at $t = 175$ s, and the initial performance is recovered in about 35 s. Then, when the UAV regains full control authority at $t = 250$ s, the UAV remains stable and eventually recovers the original performance after a transient of 50 s.

Figure 20 presents the results obtained for this experiment when the $\mathcal{L}_1$ controller is wrapped around the

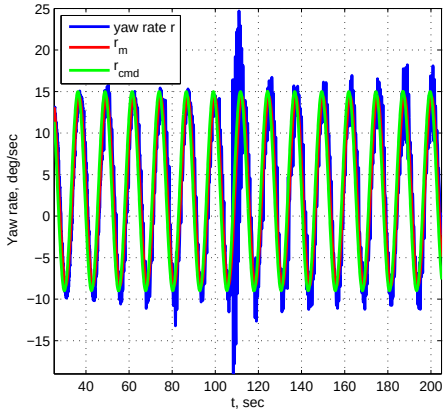

(a) Tracking performance

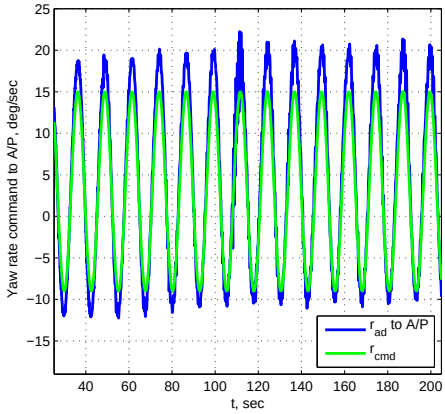

(b) Adaptive command to AP

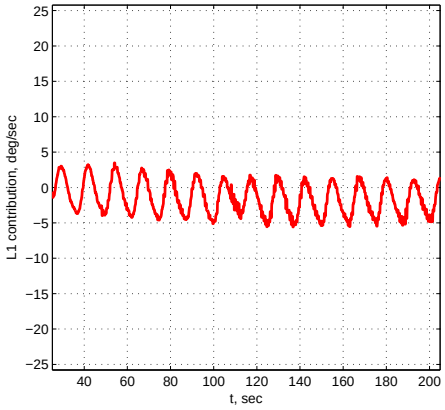

(c) $\mathcal{L}_1$ contribution

Figure 15: $\mathcal{L}_1$. Closed loop response in the presence of bending modes to a biased sinusoidal reference signal at $\omega = 0.5 \ \frac{\text{rad}}{\text{s}}$.

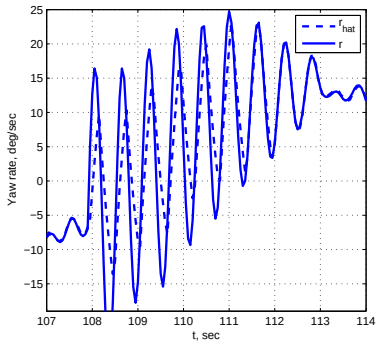

(a) Output $r(t)$ vs Predictor Output $\hat{r}(t)$

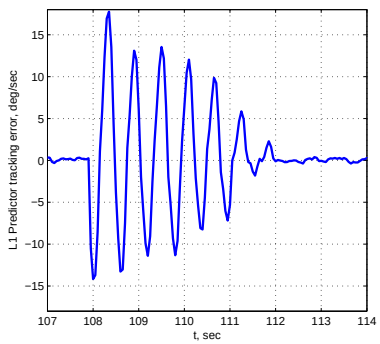

(b) Tracking error $\tilde{r}(t)$

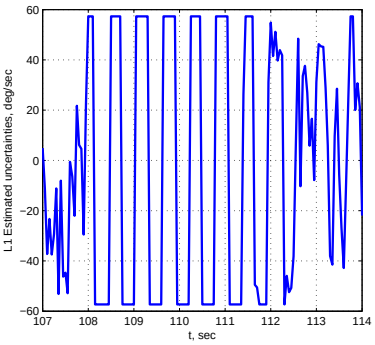

(c) uncertainty estimate $\hat{\sigma}(t)$

Figure 16: $\mathcal{L}_1$. Saturation in the adaptive law.

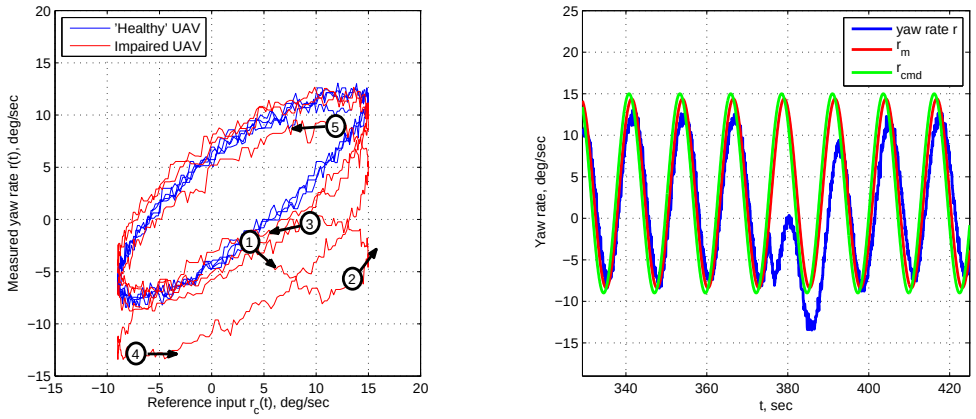

(a) Lissajous $r(r_{\text{cmd}})$ (b) Tracking performance

Figure 17: Autopilot. Response of the nominal UAV with its autopilot to a biased sinusoidal reference signal in the event of a left aileron failure.

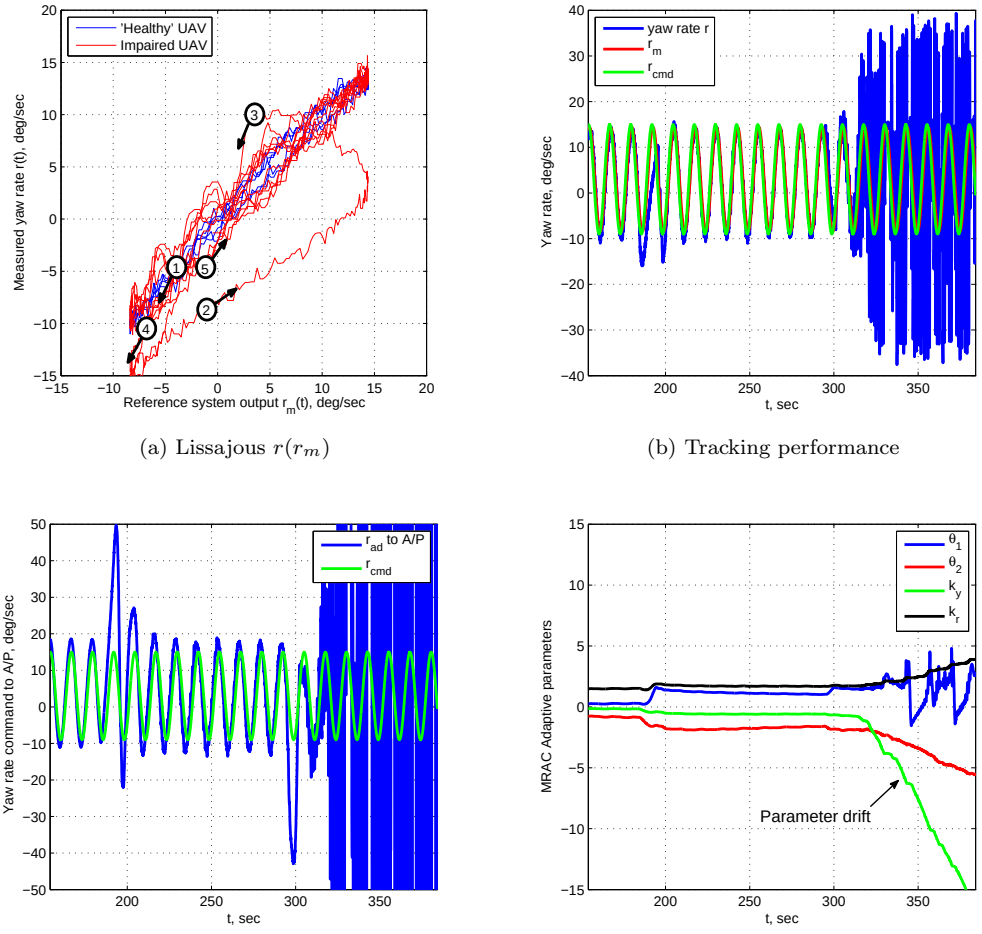

(a) Lissajous $r(r_m)$ (b) Tracking performance

(c) Adaptive command to AP (d) MRAC parameters

Figure 18: MRAC. Closed loop response to a biased sinusoidal reference signal in the event of a left aileron failure and later recovery of full control authority.

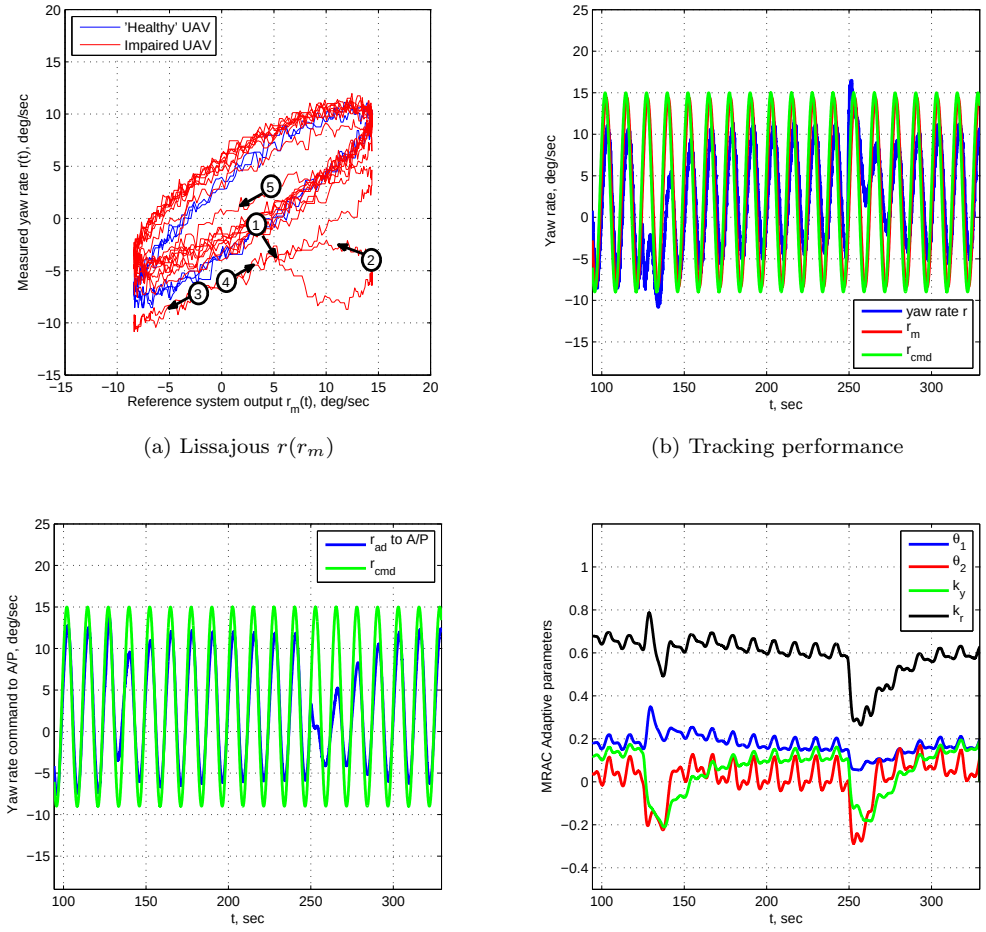

(a) Lissajous $r(r_m)$

(b) Tracking performance

(c) Adaptive command to AP

(d) MRAC parameters

Figure 19: MRAC with e–modification. Closed loop response to a biased sinusoidal reference signal in the event of a left aileron failure and later recovery of full control authority.

autopilot. The failure is introduced at $t = 100$ s and the $\mathcal{L}_1$ adaptive controller takes 15 s to regain the original level of performance using the remaining control authority. Note that even though the UAV has recovered the desired performance in 15 s, the integrators inside the AP keep readjusting during approximately 15 more seconds, and therefore the contribution of the $\mathcal{L}_1$ adaptive controller also has to readjust accordingly. The Lissajous curve shows that the $\mathcal{L}_1$ adaptive controller is able to maintain the initial phase shift of the output of the plant with respect to the output of the reference system, while the gain slightly increases for the impaired UAV. When the UAV regains full control authority at $t = 170$ s, the closed loop adaptive system is able to stabilize the plant and achieve desired performance in again 15 s. After 15 more seconds, when the integrators inside the AP readjust, the adaptive command of the $\mathcal{L}_1$ controller to the autopilot is the same as it was for the initial "healthy" UAV. Note that the transient characteristics of the closed loop adaptive system when (i) the failure is introduced, and (ii) the UAV regains full control authority, are similar. This consistent behavior of the $\mathcal{L}_1$ adaptive controller, which can be extended to the steady state regime as well, has been observed in several other similar simulations, and results in a predictable response of the closed loop adaptive system.

To conclude this experiment, Figure 21 shows a set of three Lissajous figures obtained by plotting the adaptive command sent to the autopilot against the reference signal. These figures illustrate the way the three different adaptive controllers modify the biased sinusoidal reference signal to achieve the desired tracking performance. In Figure 21a, one can see that some oscillations appear in the command the MRAC algorithm sends to the autopilot for the impaired UAV, and eventually the system becomes unstable when full control

authority is recovered. When the MRAC algorithm is implemented with the e–modification, the contribution of the adaptive controller does not change significantly during the whole experiment (see Figure 21b), which makes evident that this modification of the adaptive law limits the capabilities of the MRAC algorithm to improve the transient characteristics and recover desired system performance. Finally, Figure 21c shows the contribution of the $\mathcal{L}_1$ adaptive controller. During the transient phase, the adaptive controller contributes significantly in order to stabilize the plant and track the output of the reference system with the available control authority, while guaranteeing a smooth recovery. Eventually, when the integrators in the autopilot readjust and are able to compensate for the failure, the command from the adaptive controller converges to the initial contribution. This Figure 21c also shows that the contribution of the $\mathcal{L}_1$ controller is slightly greater for the impaired UAV in order to compensate for the reduction in control authority.

B. Flight Test Results

1. Nominal Adaptive Loop Performance

Before reproducing Rohrs' simulations in actual flight tests, we first need to verify the robustness and performance characteristics of the adaptive augmentation loops designed in the HIL simulation environment for the nominal plant consisting of the UAV with its autopilot. To this end, a series of flight tests with the different adaptive controllers were performed in which the closed loop adaptive system was driven by a biased sinusoidal reference signal of amplitude 7 $\frac{\text{deg}}{\text{s}}$ at different frequencies.

Figures 22 and 23 present the results obtained in two of these experiments. Both algorithms achieve satisfactory performance, with responses comparable to the ones obtained in HIL simulation. The existence of turbulence makes the quality of the data acquired in flight poorer than in HIL simulation. It is important to mention that, even for the nominal plant without artificially injected unmodeled dynamics, the MRAC parameters slowly diverge. In flight with the $\mathcal{L}_1$ adaptive controller, one can observe that at $t = 70$ s the $\mathcal{L}_1$ adaptive controller generates small oscillations at an approximate frequency of 1 Hz in the control channel for approximately 3 s. Again, these oscillations are due to internal saturation of the $\mathcal{L}_1$ controller. The levels of the projection operator were too tight for the level of turbulence encountered during flight. Nevertheless, stability of the closed loop adaptive system was not compromised.

2. Second Order Unmodeled Dynamics

During the flight tests, the same second order transfer function considered in Section IV.A.1, with natural frequency $\omega_n = 1.5$ $\frac{\text{rad}}{\text{s}}$ and damping ratio $\zeta = 0.45$, was "injected" at the output of the actual plant. Using the Lissajous curves, the phase crossover frequency of the real plant with the unmodeled dynamics was determined in real time with data received through telemetry on the ground. Figure 24 shows the Lissajous curve $r(r_{\text{cmd}})$ for the system driven by a biased sinusoidal reference signal at $\omega = 1.6$ $\frac{\text{rad}}{\text{s}}$; one can see that, similar to the experiments in HIL simulation environment, this Lissajous curve presents a phase shift of -180 deg between the reference signal and the output of the system.

Next, we need to verify that we are able to reproduce in real flight the same instability phenomena observed in HIL simulation. To this end, the system with unmodeled dynamics and the conventional MRAC algorithm is driven by a biased sinusoidal reference signal at the phase crossover frequency. Figure 25 shows the response of the closed loop adaptive system. One can see that the parameters drift slowly, generating adaptive command signals larger than ± 100 $\frac{\text{deg}}{\text{s}}$. This same experiment was repeated for different values of the adaptive gains. The objective was to analyze the sensitivity of the robustness of the closed loop adaptive system to the rate of adaptation. Figure 26 shows the response of the system to the same reference signal with adaptive gains 1.5 times larger than the original ones. After an initial slow drift, the parameters blow up at $t = 110$ s. This result is consistent with MRAC theory: as one tries to increase the speed of adaptation, the robustness margins of the adaptive system decrease.

The same experiment (with the original adaptive gains) was conducted for the MRAC algorithm with the e–modification (see Figure 27). As expected, the parameters do not drift, and the system retains stability during the whole flight. However, similar to HIL results, the performance of the closed loop adaptive system is significantly degraded due to the addition of the damping term in the adaptive law. In this sense, the closed loop adaptive system is not even able to track the DC component of the reference signal.

Finally, in Figure 28, we present flight test results obtained for the $\mathcal{L}_1$ adaptive augmentation. The system maintains stability during the whole flight and the control signal remains inside reasonable bounds during the experiment. As one would expect, since the frequency of the reference signal is well beyond

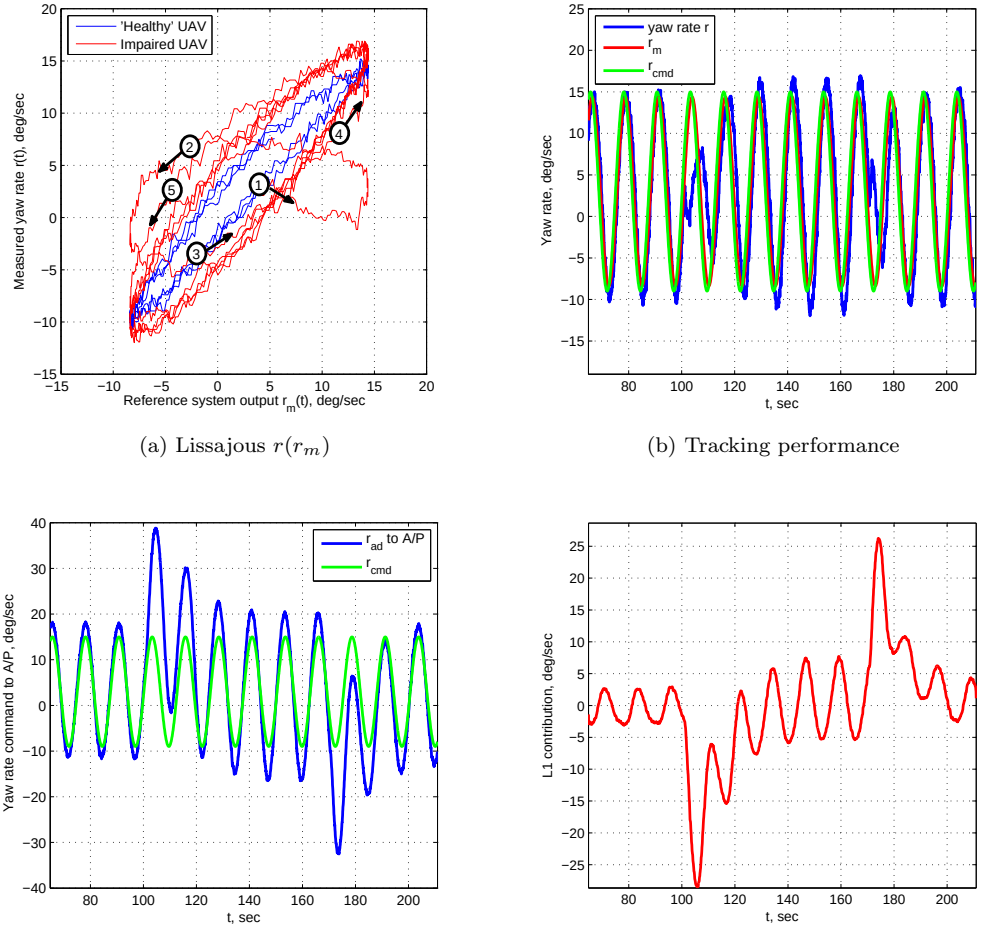

(a) Lissajous $r(r_m)$

(b) Tracking performance

(c) Adaptive command to AP

(d) $\mathcal{L}_1$ contribution

Figure 20: $\mathcal{L}_1$. Closed loop response to a biased sinusoidal reference signal in the event of a left aileron failure and later recovery of full control authority.

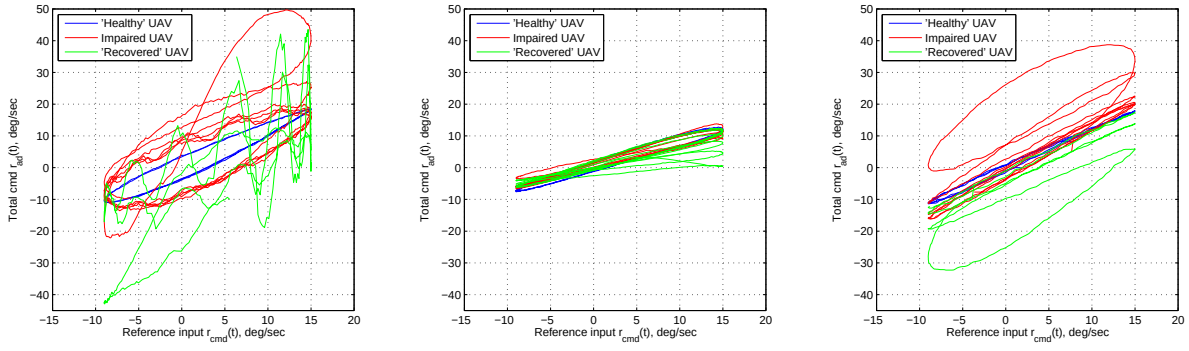

(a) MRAC

(b) MRAC with ϵ-modification

(c) $\mathcal{L}_1$ adaptive controller

Figure 21: Lissajous $r_{\text{ad}}(r_{\text{cmd}})$ for the three different adaptive controllers in response to a biased sinusoidal reference signal, and in the event of a left aileron failure and later recovery of full control authority.

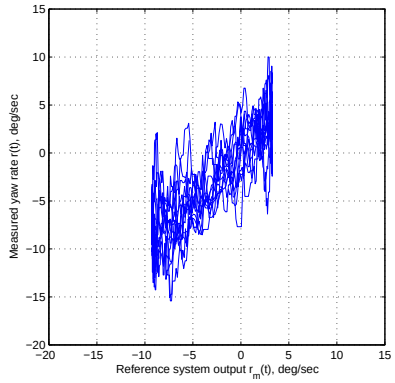

(a) Lissajous $r(r_m)$

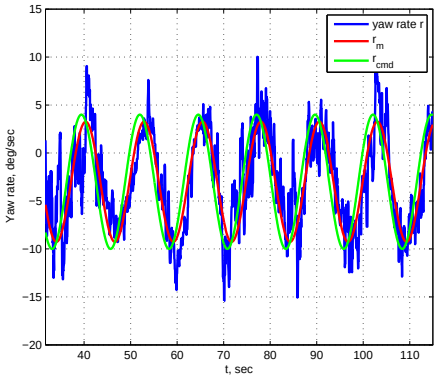

(b) Tracking performance

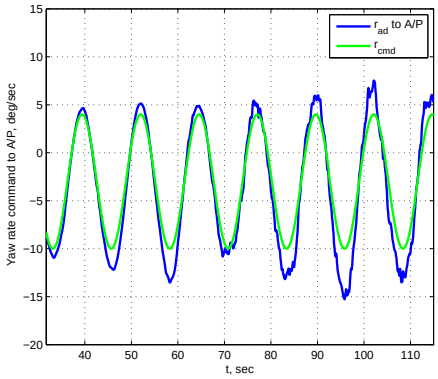

(c) Adaptive command to AP

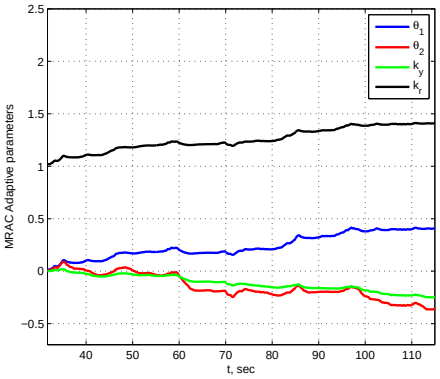

(d) MRAC parameters

Figure 22: MRAC. Closed loop nominal response to a biased sinusoidal reference signal at $\omega = 0.5$ $\frac{\text{rad}}{\text{s}}$.

the bandwidth of the low pass filter $C(s)$ in the control law (which was set to 0.6 $\frac{\text{rad}}{\text{s}}$), the $\mathcal{L}_1$ adaptive controller is not able to achieve desired performance. We note, nevertheless, that the closed loop system with the $\mathcal{L}_1$ adaptive controller is able to track the bias term of the reference signal, which suggests that the $\mathcal{L}_1$ adaptive augmentation ensures tracking of the low frequency content of the reference signal while guaranteeing stability of the system to its high frequency content. Furthermore, Figure 29 illustrates the graceful degradation of performance with the $\mathcal{L}_1$ adaptive controller as the frequency of the reference signal increases beyond the bandwidth of the low pass filter. In this set of experiments, the closed loop system with the second order unmodeled dynamics and the $\mathcal{L}_1$ adaptive controller was driven by biased sinusoidal reference signals at different frequencies. It can be seen that the output of the closed loop adaptive system is able to track the output of the reference system for reference signals at low frequencies ($\omega = 0.3$ $\frac{\text{rad}}{\text{s}}$), and, as the frequency of the reference signal increases, the eccentricity of the Lissajous curve decreases. This graceful degradation in the performance of the system is consistent with the theory of fast and robust adaptation, and results in a predictable response of the closed loop adaptive system, in contrast to MRAC algorithms.

To conclude this section, we present a last set of figures (Figures 30a and 30b) which demonstrate the recovery capabilities of the $\mathcal{L}_1$ adaptive control system. The experiment starts with the nominal plant consisting of the UAV and its autopilot driven by a sinusoidal reference signal at 1.6 $\frac{\text{rad}}{\text{s}}$. The second order unmodeled dynamics are then injected and, since 1.6 $\frac{\text{rad}}{\text{s}}$ corresponds to the phase crossover frequency of the system with unmodeled dynamics, the Lissajous figure adopts the typical shape for -180 deg of phase shift. When the MRAC is enabled, the closed loop system becomes unstable as expected, and the control command from the adaptive algorithm starts growing and eventually hits the saturation limit of the autopilot. Then, at $t = 56$ s, the $\mathcal{L}_1$ adaptive controller is engaged and the UAV recovers stability in around 1.5 s, thus confirming the theoretical claims of fast and and robust adaptation.

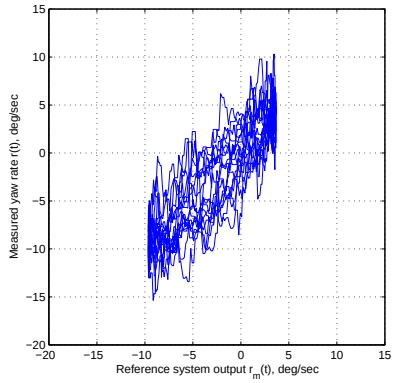

(a) Lissajous $r(r_m)$

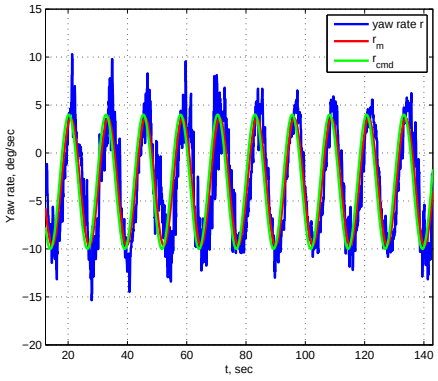

(b) Tracking performance

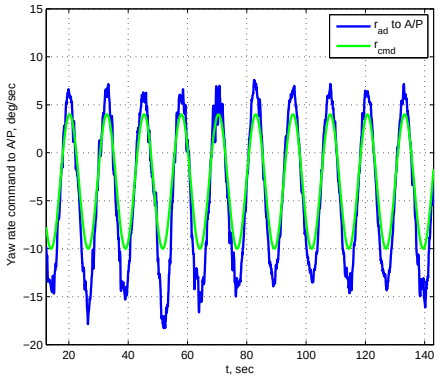

(c) Adaptive command to AP

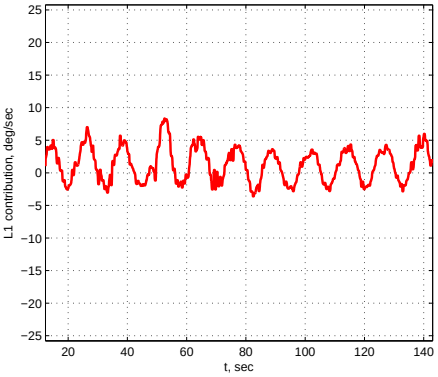

(d) $\mathcal{L}_1$ contribution

Figure 23: $\mathcal{L}_1$. Closed loop nominal response to a biased sinusoidal reference signal at $\omega = 0.5$ $\frac{\text{rad}}{\text{s}}$.

V. Conclusions

This paper presented new results on the verification and in–flight validation of an $\mathcal{L}_1$ adaptive flight control system. The paper also proposed a general methodology for safe verification and validation of adaptive flight control systems, consisting in the artificial "injection" of different unmodeled dynamics and real–time monitoring of the system response to reference inputs of different amplitudes and frequencies. To keep the results in historical perspective, the proposed framework is based on Rohrs' counterexample, presented in the early 80s to show the limitations of adaptive controllers developed at that time. The current framework allows to evaluate the performance and robustness of the closed loop adaptive system in the presence of general unmodeled dynamics. A detailed analysis of HIL simulations and flight test results are included in the paper. This analysis demonstrated the lack of predictability of conventional MRAC algorithms and showed that this class of adaptive algorithms loses stability in the presence of unmodeled dynamics, thus verifying that the flight test setup adopted qualitatively reproduces the results obtained by Rohrs and coauthors. In addition, it was shown that the damping type modifications in the adaptive laws proposed in the literature retain stability of the closed loop adaptive system, introducing however a significant degradation in the tracking capabilities of the closed loop system.

Finally, the $\mathcal{L}_1$ output feedback adaptive controller was also flight tested in the same setup. Both HIL simulations and flight test results confirmed that the $\mathcal{L}_1$ controller maintains stability and predictable performance in the presence of unmodeled dynamics and control surface failures, and thus solves the problem that Rohrs and coauthors posed regarding performance and robustness of the standard adaptive architectures. In $\mathcal{L}_1$ adaptive control architectures, robustness of the closed loop adaptive system is ensured by the low pass filter inserted in the control law, while fast adaptation results in a predictable and consistent closed loop performance. This separation between adaptation and robustness, which is the key feature of $\mathcal{L}_1$ adaptive

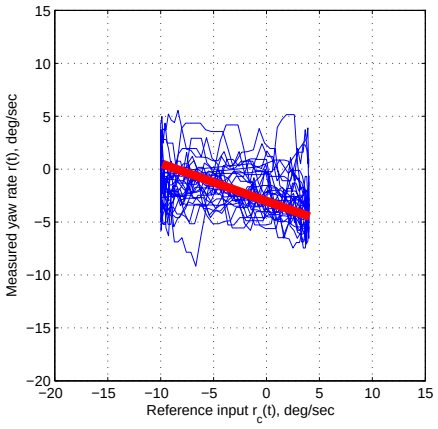

Figure 24: Lissajous curve for the nominal system with unmodeled dynamics at the phase crossover frequency ($\omega = 1.6\ \frac{\text{rad}}{\text{s}}$).

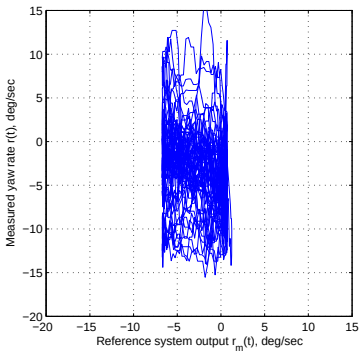

(a) Lissajous $r(r_m)$

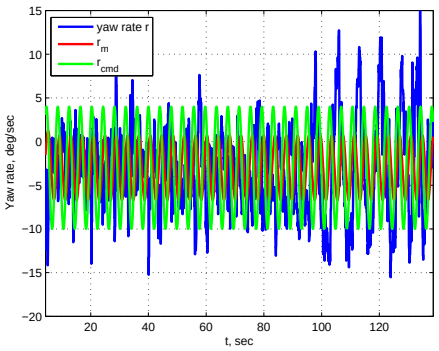

(b) Tracking performance

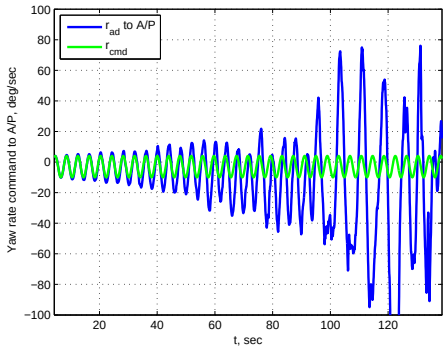

(c) Adaptive command to AP

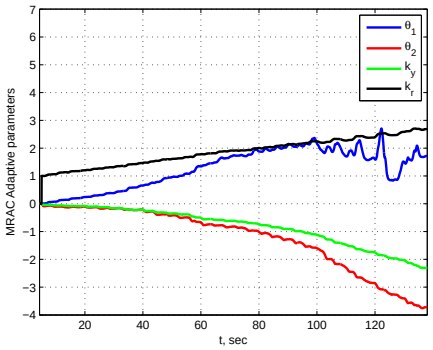

(d) MRAC parameters

Figure 25: MRAC. Closed loop nominal response in the presence of second order unmodeled dynamics to a biased sinusoidal reference signal at the phase crossover frequency ($\omega = 1.6\ \frac{\text{rad}}{\text{s}}$).

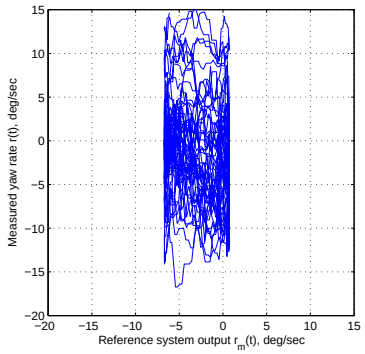

(a) Lissajous $r(r_m)$

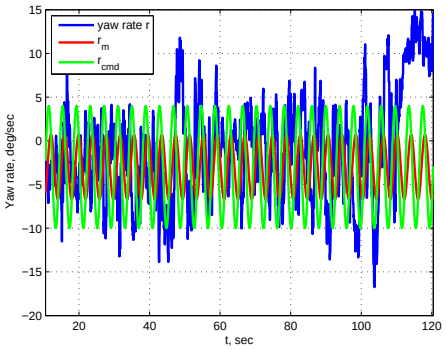

(b) Tracking performance

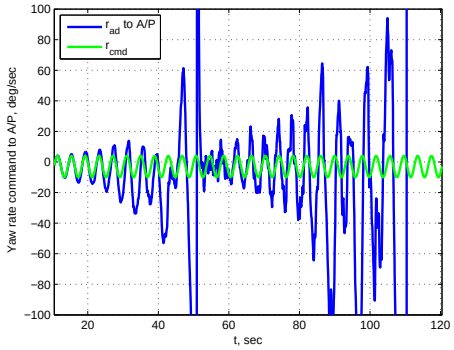

(c) Adaptive command to AP

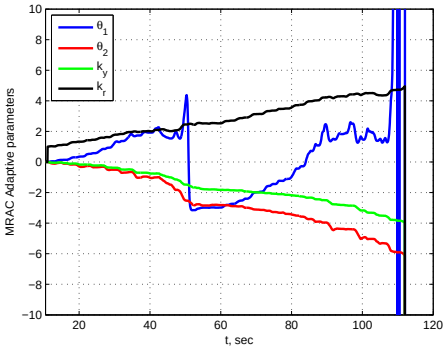

(d) MRAC parameters

Figure 26: MRAC. Closed loop nominal response in the presence of second order unmodeled dynamics to a biased sinusoidal reference signal at the phase crossover frequency ($\omega = 1.6\ \frac{\text{rad}}{\text{s}}$) with higher adaptation rate.

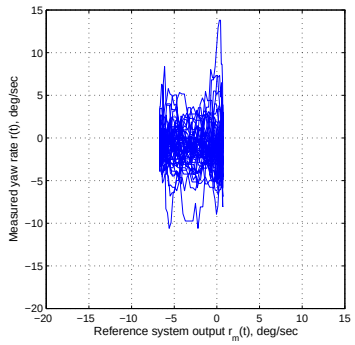

(a) Lissajous $r(r_m)$

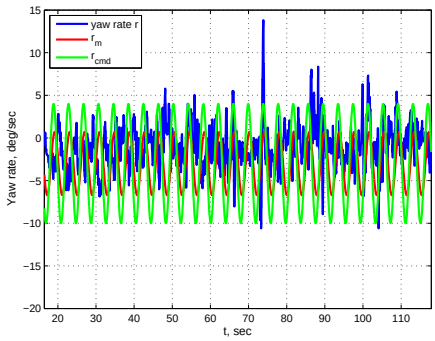

(b) Tracking performance

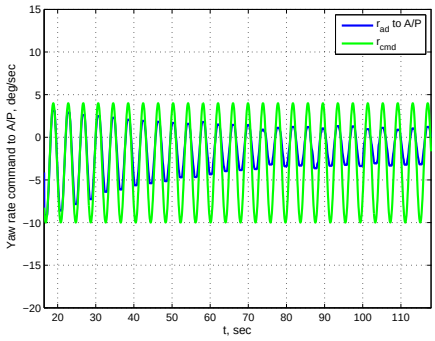

(c) Adaptive command to AP

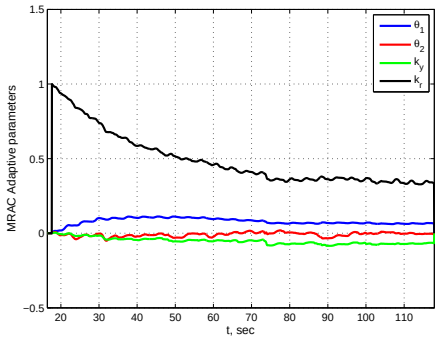

(d) MRAC parameters

Figure 27: MRAC with e–modification. Closed loop nominal response in the presence of second order unmodeled dynamics to a biased sinusoidal reference signal at the phase crossover frequency ($\omega = 1.6\ \frac{\text{rad}}{\text{s}}$).

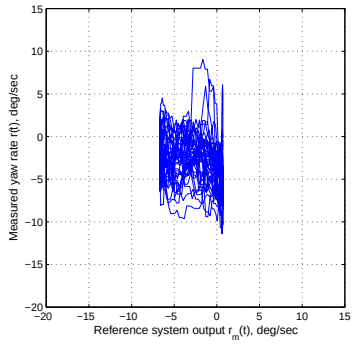

(a) Lissajous $r(r_m)$

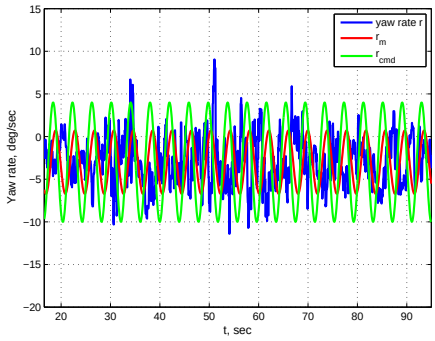

(b) Tracking performance

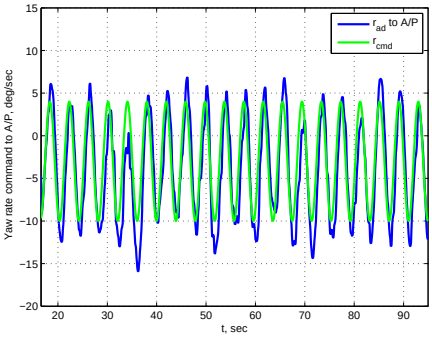

(c) Adaptive command to AP

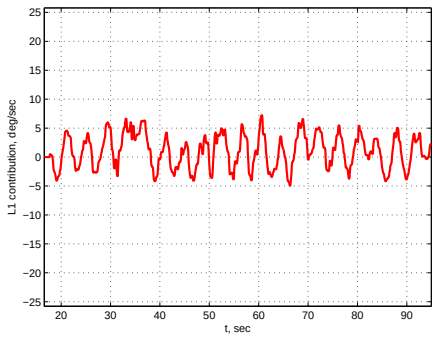

(d) $\mathcal{L}_1$ contribution

Figure 28: $\mathcal{L}_1$. Closed loop nominal response in the presence of second order unmodeled dynamics to a biased sinusoidal reference signal at the phase crossover frequency ($\omega = 1.6\ \frac{\text{rad}}{\text{s}}$).

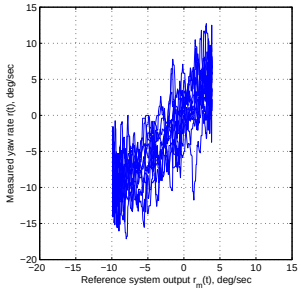

(a) Lissajous $r(r_m)$

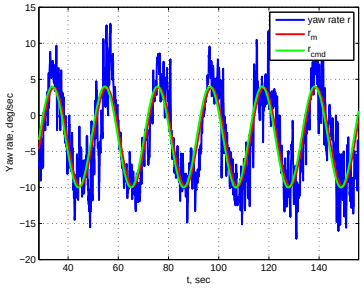

(b) Tracking performance

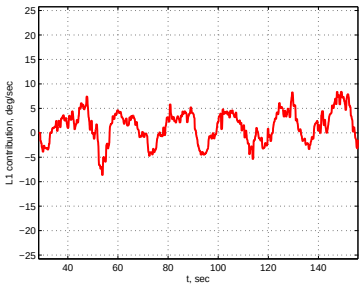

(c) $\mathcal{L}_1$ contribution

Figure 29: $\mathcal{L}_1$. Closed loop response in the presence of second order unmodeled dynamics to biased sinusoidal reference signal at $\omega = 0.3$ $\frac{\text{rad}}{\text{s}}$.

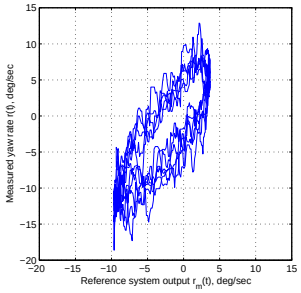

(d) Lissajous $r(r_m)$

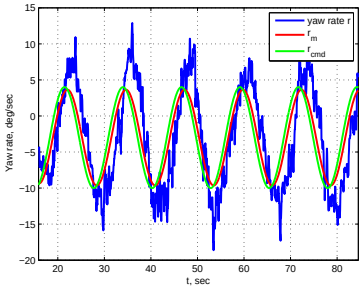

(e) Tracking performance

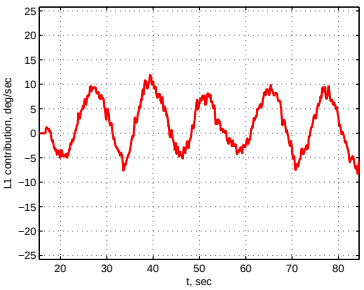

(f) $\mathcal{L}_1$ contribution

Figure 29: $\mathcal{L}_1$. Closed loop response in the presence of second order unmodeled dynamics to biased sinusoidal reference signal at $\omega = 0.5$ $\frac{\text{rad}}{\text{s}}$.

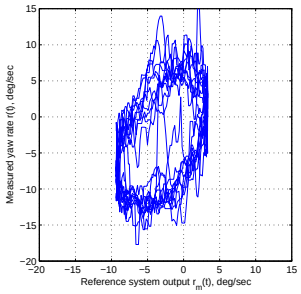

(g) Lissajous $r(r_m)$

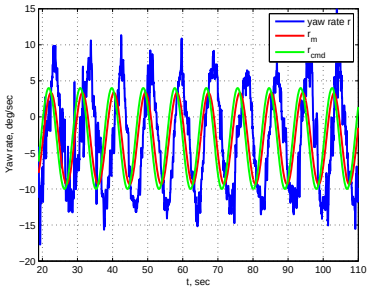

(h) Tracking performance

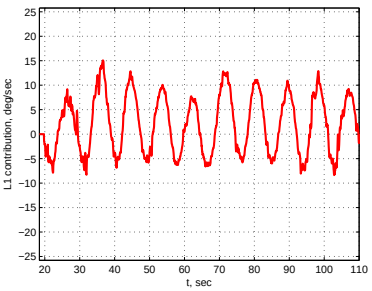

(i) $\mathcal{L}_1$ contribution

Figure 29: $\mathcal{L}_1$. Closed loop response in the presence of second order unmodeled dynamics to biased sinusoidal reference signal at $\omega = 0.7$ $\frac{\text{rad}}{\text{s}}$.

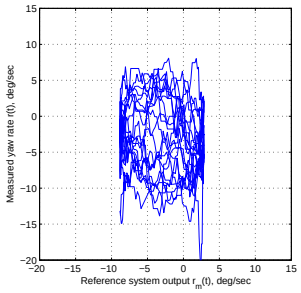

(j) Lissajous $r(r_m)$

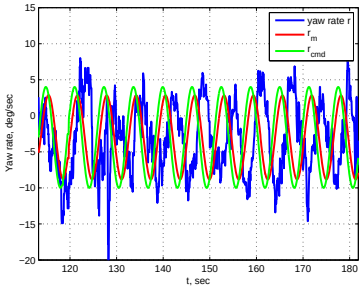

(k) Tracking performance

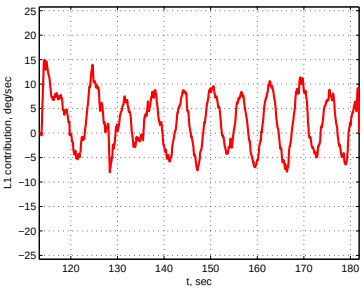

(l) $\mathcal{L}_1$ contribution

Figure 29: $\mathcal{L}_1$. Closed loop response in the presence of second order unmodeled dynamics to biased sinusoidal reference signal at $\omega = 1.0$ $\frac{\text{rad}}{\text{s}}$.

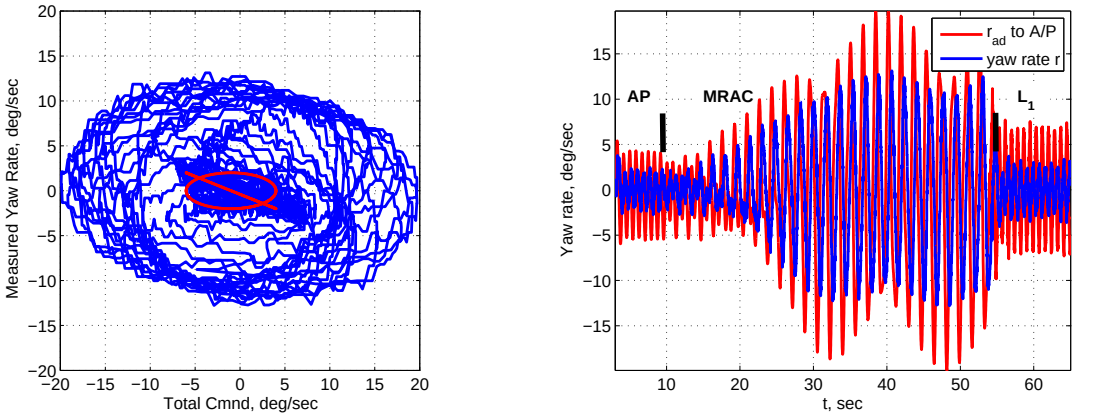

(a) Lissajous $r(r_{\text{ad}})$

(b) Adaptive command to AP and turn rate response

Figure 30: MRAC and $\mathcal{L}_1$ algorithms in flight reproducing Rohrs' setup.

control, is in contrast to the current prevailing "conventional" wisdom, that slow adaptation was indicated so that robustness would not be compromised. The results in this paper illustrate the features of $\mathcal{L}_1$ adaptive control theory and demonstrate the advantages of $\mathcal{L}_1$ architectures as *verifiable* robust adaptive control architectures with the potential of reducing flight control design costs and facilitating the transition of adaptive control into advanced flight control systems.

VI. Acknowledgments

This work was sponsored in part by NASA Grants NNX08AB97A, NNX08AC81A, and NNL08AA12I.

References

[1]Jacklin, S. A., Lowry, M. R., Schumann, J. M., Gupta, P. P., Bosworth, J. T., Zavala, E., Kelly, J. W., Hayhurst, K. J., Belcastro, C. M., and Belcastro, C. M., "Verification, Validation, and Certification Challenges for Adaptive Flight-Critical Control System Software," *AIAA Guidance, Navigation and Control Conference*, Providence, RI, August 2004, AIAA-2004-5258.

[2]Jacklin, S. A., "Closing Certification Gaps in Adaptive Flight Control Software," *AIAA Guidance, Navigation and Control Conference*, Honolulu, HI, August 2008, AIAA-2008-6988.

[3]Egardt, B., *Stability of Model Reference Adaptive and Self–Tuning Regulators*, Ph.D. thesis, Lund Institute of Technology, December 1978.

[4]Rohrs, C. E., Valavani, L. S., Athans, M., and Stein, G., "Robustness of Adaptive Control Algorithms in the Presence of Unmodeled Dynamics," *IEEE Conference on Decision and Control*, Vol. 1, Orlando, FL, December 1982, pp. 3–11.

[5]Rohrs, C. E., Valavani, L. S., Athans, M., and Stein, G., "Robustness of Continuous-Time Adaptive Control Algorithms in the Presence of Unmodeled Dynamics," *IEEE Transactions on Automatic Control*, Vol. 30, No. 9, September 1985, pp. 881–889.

[6]Georgiou, T. T. and Smith, M. C., "Robustness Analysis of Nonlinear Feedback Systems: An Input-Output Approach," *IEEE Transactions on Automatic Control*, Vol. 42, No. 9, September 1997, pp. 1200–1221.

[7]Anderson, B. D. O., "Adaptive Systems, Lack of Persistency of Excitation and Bursting Phenomena," *Automatica*, Vol. 21, No. 3, May 1985, pp. 247–258.

[8]Mareels, I. M. Y. and Bitmead, R. R., "Non–linear Dynamics in Adaptive Control: Chaotic and Periodic Stabilization," *Automatica*, Vol. 22, No. 6, November 1986, pp. 641–655.

[9]Aloneftis, A., *Stochastic Adaptive Control: Results and Simulations*, Vol. 98 of *Lecture Notes in Control and Information Sciences*, Springer-Verlag New York, Inc., New York, NY, 1987.

[10]Kosut, R. L., Mareels, I. M. Y., Anderson, B. D. O., Bitmead, R. R., and Johnson, Jr., C. R., "Transient Analysis of Adaptive Control," *IFAC World Congress*, Munich, Federal Republic of Germany, July 1987, pp. 121–126.

[11]Mareels, I. M. Y. and Bitmead, R. R., "Non–linear Dynamics in Adaptive Control: Chaotic and Periodic Stabilization—II. Analysis," *Automatica*, Vol. 24, No. 4, July 1988, pp. 485–497.

[12]Zang, Z. and Bitmead, R. R., "Transient Bounds for Adaptive Control Systems," *IEEE Conference on Decision and Control*, Vol. 5, Honolulu, HI, December 1990, pp. 2724–2729.

[13]Zang, Z. and Bitmead, R. R., "Transient Bounds for Adaptive Control Systems," *IEEE Transactions on Automatic Control*, Vol. 39, No. 1, January 1994, pp. 171–175.

[14]Åström, K. J., "Analysis of Rohrs Counterexamples to Adaptive Control," *IEEE Conference on Decision and Control*, San Antonio, TX, December 1983, pp. 982–987.

[15]Åström, K. J., "Interactions between Excitation and Unmodeled Dynamics in Adaptive Control," *IEEE Conference on Decision and Control*, Las Vegas, NV, December 1984, pp. 1276–1281.

[16]Anderson, B. D. O., "Failures of Adaptive Control Theory and their Resolution," *Communications in Information and Systems*, Vol. 5, No. 1, 2005, pp. 1–20.

[17]Ioannou, P. A. and Kokotović, P. V., "An Asymptotic Error Analysis of Identifiers and Adaptive Observers in the Presence of Parasitics," *IEEE Transactions on Automatic Control*, Vol. 27, No. 4, August 1982, pp. 921–927.

[18]Peterson, B. B. and Narendra, K. S., "Bounded Error Adaptive Control," *IEEE Transactions on Automatic Control*, Vol. 27, No. 6, December 1982, pp. 1161–1168.

[19]Kresselmeier, G. and Narendra, K. S., "Stable Model Reference Adaptive Control in the presence of Bounded Disturbances," *IEEE Transactions on Automatic Control*, Vol. 27, No. 6, December 1982, pp. 1169–1175.

[20]Ioannou, P. A. and Kokotović, P. V., *Adaptive Systems with Reduced Models*, Springer-Verlag New York, Inc., Secaunus, NJ, 1983.

[21]Ioannou, P. A. and Kokotović, P. V., "Robust Redesign of Adaptive Control," *IEEE Transactions on Automatic Control*, Vol. 29, No. 3, March 1984, pp. 202–211.

[22]Narendra, K. S. and Annaswamy, A. M., "A New Adaptive Law for Robust Adaptation Without Persistent Excitation," *IEEE Transactions on Automatic Control*, Vol. 32, No. 2, February 1987, pp. 134–145.

[23]Ortega, R. and Tang, Y., "Robustness of Adaptive Controllers—A Survey," *Automatica*, Vol. 25, No. 5, September 1989, pp. 651–677.

[24]Cao, C., Patel, V. V., Reddy, C. K., Hovakimyan, N., Lavretsky, E., and Wise, K. A., "Are Phase and Time-delay Margins Always Adversely Affected by High-Gain?" *AIAA Guidance, Navigation and Control Conference*, Keystone, CO, August 2006, AIAA-2006-6347.

[25]Cao, C. and Hovakimyan, N., "Design and Analysis of a Novel $\mathcal{L}_1$ Adaptive Control Architecture with Guaranteed Transient Performance," *IEEE Transactions on Automatic Control*, Vol. 53, No. 2, March 2008, pp. 586–591.

[26]Cao, C. and Hovakimyan, N., "Stability Margins of $\mathcal{L}_1$ Adaptive Control Architecture," *IEEE Transactions on Automatic Control*, Vol. 55, No. 2, February 2010.

[27]Dobrokhodov, V., Yakimenko, O., Jones, K. D., Kaminer, I., Bourakov, E., Kitsios, I., and Lizarraga, M., "New Generation of Rapid Flight Test Prototyping System for Small Unmanned Air Vehicles," *Proc. of AIAA Modelling and Simulation Technologies Conference*, Hilton Head Island, SC, August 2007, AIAA-2007-6567.

[28]Cao, C. and Hovakimyan, N., "$\mathcal{L}_1$ Adaptive Output Feedback Controller for Systems of Unknown Dimension," *IEEE Transactions on Automatic Control*, Vol. 53, No. 3, April 2008, pp. 815–821.

[29]Cao, C. and Hovakimyan, N., "$\mathcal{L}_1$ Adaptive Output-Feedback Controller for Non-Stricly-Positive-Real Reference Systems: Missile Longitudinal Autopilot Design," *AIAA Journal of Guidance, Control, and Dynamics*, Vol. 32, No. 3, May-June 2009, pp. 717–726.

[30]Dobrokhodov, V., Kitsios, I., Kaminer, I., Jones, K. D., Xargay, E., Hovakimyan, N., Cao, C., Lizárraga, M. I., and Gregory, I. M., "Flight Validation of Metrics Driven $\mathcal{L}_1$ Adaptive Control," *AIAA Guidance, Navigation and Control Conference*, Honolulu, HI, August 2008, AIAA-2008-6987.

[31]Cundy, H. M. and Rollett, A. P., *Mathematical Models*, Oxford University Press, London, UK, 1961.

[32]Michini, B. and How, J., "$\mathcal{L}_1$ Adaptive Control for Indoor Autonomous Vehicles: Design Process and Flight Testing," *AIAA Guidance, Navigation and Control Conference*, Chicago, IL, August 2009, AIAA-2009-5754.

[33]Narendra, K. S. and Annaswamy, A. M., *Stable Adaptive Systems*, Information and System Sciences, Prentice Hall, Englewood Cliffs, NJ, 1989.

[34]Ioannou, P. A. and Sun, J., *Robust Adaptive Control*, Prentice Hall, Upper Saddle River, NJ, 1996.

[35]Pomet, J.-B. and Praly, L., "Adaptive nonlinear regulation: Estimation from the Lyapunov Equation," *IEEE Transactions on Automatic Control*, Vol. 37, No. 6, June 1992, pp. 729–740.